ELSEVIER

Neurobiology of Aging 33 (2012) 1011.e11–1011.e23

NEUROBIOLOGY OF AGING

www.elsevier.com/locate/neuaging

Environmental enrichment ameliorated high-fat diet-induced Aβ deposition and memory deficit in APP transgenic mice

Masato Maesako[a], Kengo Uemura[b], Masakazu Kubota[a], Akira Kuzuya[b], Kazuki Sasaki[a], Megumi Asada[a], Kiwamu Watanabe[b], Naoko Hayashida[a], Masafumi Ihara[b], Hidefumi Ito[b], Shun Shimohama[c], Takeshi Kihara[a], Ayae Kinoshita[a,*]

[a] *School of Human Health Sciences, Kyoto University Graduate School of Medicine, Kyoto 606-8507, Japan*
[b] *Department of Neurology, Kyoto University Graduate School of Medicine, Kyoto 606-8507, Japan*
[c] *Department of Neurology, Sapporo Medical University, Sapporo 060-8556, Japan*

Received 21 May 2011; received in revised form 4 August 2011; accepted 24 October 2011

Abstract

The pathogenesis of Alzheimer's disease (AD) is tightly associated with metabolic dysfunctions. In particular, a potential link between type 2 diabetes (T2DM) and AD has been suggested epidemiologically, clinically, and experimentally, and some studies have suggested that exercise or dietary intervention reduces risk of cognitive decline. However, there is little solid molecular evidence for the effective intervention of metabolic dysfunctions for prevention of AD. In the present study, we established the AD model mice with diabetic conditions through high-fat diet (HFD) to examine the effect of environmental enrichment (EE) on HFD-induced AD pathophysiology. Here, we demonstrated that HFD markedly deteriorated memory impairment and increased β-amyloid (Aβ) oligomers as well as Aβ deposition in amyloid precursor protein (APP) transgenic mice, which was reversed by exposure to an enriched environment for 10 weeks, despite the continuation of HFD. These studies provide solid evidence that EE is a useful intervention to ameliorate behavioral changes and AD pathology in HFD-induced aggravation of AD symptoms in APP transgenic mice.

Keywords: Alzheimer's disease; Type 2 diabetes; High-fat diet; Environmental enrichment; β-Amyloid

1. Introduction

Alzheimer's disease (AD), the most common cause of dementia, is poised to become a significant public health crisis. The occurrence of AD is largely sporadic, typically affecting individuals over 65 years, but a minority of the cases (5%) display familial inheritance with early onset. One of the pathological hallmarks of AD is amyloid plaques. Amyloid plaques are composed of 40–42-residue peptides, called β-amyloid (Aβ) (designated as Aβ40, Aβ42), which are derived from the amyloid precursor protein (APP) via proteolytic cleavages by β- and γ-secretases. Presenilin 1 and presenilin 2 (PS1 and PS2) are known to be the catalytic core of γ-secretase (De Strooper et al., 1998). A widely accepted hypothesis about AD pathogenesis is that Aβ production plays a crucial role in neurodegeneration (Finder, 2010). This hypothesis is supported by the discovery of causative mutations in the genes encoding APP, PS1, and PS2, in early-onset familial AD (Bertram and Tanzi, 2008; Tandon et al., 2000). Moreover, recent studies have implied small soluble Aβ oligomers, such as dimers, trimers, and dodecamers, formed during Aβ aggregation, as being the main culprits of Aβ toxicity and AD pathogenesis (Hartley et al., 1999; Lesné et al., 2006; Shankar et al., 2008; Walsh et al., 2002).

A potential link between type 2 diabetes (T2DM) and AD has been suggested by epidemiological and clinical

* Corresponding author at: School of Human Health Sciences, Kyoto University Graduate School of Medicine, 53, Shogoinkawahara-cho, Sakyo-ku, Kyoto 606-8507, Japan. Tel.: +81 75 751 3969; fax: +81 75 751 3969.

E-mail address: akinoshita@hs.med.kyoto-u.ac.jp (A. Kinoshita).

0197-4580/$ – see front matter © 2012 Elsevier Inc. All rights reserved.
doi:10.1016/j.neurobiolaging.2011.10.028

studies (Biessels et al., 2006; Ott et al., 1999). Recent experimental studies support this linkage. For example, APP-ob/ob mice, produced by crossing APP transgenic (Tg) mice with diabetic model mice, manifested earlier onset of cognitive dysfunction than APP Tg mice (Takeda et al., 2010). Moreover, using dietary interventions such as high-fat diet (HFD) or sucrose water for APP Tg mice exacerbated their memory deficits and pathological alterations in the brain (Cao et al., 2007; Ho et al., 2004). On the other hand, insulin and the insulin-sensitizing drug have been shown to improve cognitive performance in mouse models of AD, as well as in patients with early AD (Pedersen et al., 2006; Reger et al., 2008; Watson et al., 2005). These reports clearly indicate that there is an association of diabetes with a higher risk of sporadic AD. However, the impact of nonpharmacological or preventive intervention targeting AD with diabetes has not been clearly demonstrated so far.

Exercise is beneficial in the prevention and treatment of T2DM, both in human and rodent models (Cotman and Berchtold, 2007; Keller et al., 1993; Sanz et al., 2010). In the environmental enrichment (EE) condition, mice are allowed the freedom to move and exercise voluntarily in the larger cage, with accessibility to complex stimuli (e.g. toys, running wheels), thus being provided with more physical and intellectual stimulation than mice housed in standard laboratory conditions. In the AD research fields, some reports demonstrated that EE applied to AD model mice reduced Aβ deposition, enhanced synaptic plasticity, and ameliorated cognitive deficits (Hu et al., 2010; Jankowsky et al., 2005; Lazarov et al., 2005). On the other hand, other studies suggested that EE enhanced Aβ accumulation and failed to improve memory deficits in APP Tg mice with a regular diet (Cotel et al., 2012; Jankowsky et al., 2003). Thus, the effect of EE on AD pathophysiology has been controversial.

In the present study, to determine whether regular exercise affects cognitive decline, we established the AD model mice with diabetic conditions through HFD (APP-HFD mice), which were subsequently subjected to EE. To test the effect of EE, we conducted ethological, histochemical, and biochemical analyses. Here, with the use of established animal models with both conditions, we observed that the APP-HFD mice exhibited even more impaired cognitive function than control APP Tg mice fed with normal diet (control APP mice). Additionally, we demonstrated that EE not only ameliorated obesity and glucose intolerance of the APP-HFD mice but also significantly improved their cognitive function. Notably, histochemical and biochemical analyses suggested that EE ameliorated the Aβ accumulation in the brains accelerated by HFD. Also, the amount of Aβ oligomers was elevated in the cerebrum of the APP-HFD mice, which was significantly reduced by EE settings. These results clearly indicated that EE could be an effective way to ameliorate the AD progression caused by metabolic dysfunctions.

2. Methods

2.1. Animals and dietary conditions

We used human APP Tg mice overexpressing the familial AD-linked mutations bearing both the Swedish (K670N/M671L) and Indiana (V717F) mutations (APP *Swe/Ind*) (Mucke et al., 2000), which have been imported from The Jackson Laboratory (Bar Harbor, ME). APP *Swe/Ind* mice were maintained as heterozygotes, and male and female mice were housed separately. Age- and sex-matched (1:1, male/female) mice were exposed to either an established HFD (caloric composition, 60% fat, 20% carbohydrate, and 20% protein, Research Diet, Inc., Canada) or a standard diet (10% fat, 70% carbohydrate, and 20% protein, Oriental Yeast Co., Ltd., Tokyo, Japan) for 20 weeks, from 2–3 to 7–8 months of age. To examine the effect of EE on APP Tg mice fed with HFD (APP-HFD mice), the cage of the mice was changed to a 2.4 times larger one equipped with a running wheel as well as objects like stands and toys after 10 weeks of HFD (APP-HFD + EE mice). The mice spent 10 weeks in the EE condition in the presence of HFD. After the dietary manipulation, metabolic changes in these mice were analyzed, followed by the assessment of memory function through the Morris water maze test, as described later in the text. After the analysis of memory function, the brains were extracted and were cut sagitally into left and right hemispheres. The left hemisphere was fixed in 4% paraformaldehyde for histological analysis. After removing the olfactory lobe and cerebellum, the right hemisphere was rapidly frozen in liquid nitrogen for biochemical analysis. All animal experiments were performed in compliance with the Guidelines for the Care and Use of Laboratory Animals of the Kyoto University.

2.2. Assessment of metabolic changes

To assess glucose intolerance in these mice, we assessed changes in circulating glucose levels, as a function of time in response to the intraperitoneal glucose tolerance test (IGTT). Mice were given a single dose of intraperitoneal injection of glucose (2 g/kg body weight) after 14 hours of fasting, and blood was collected from the tail vein periodically over 2 hours. Blood glucose content was measured by using LabAssay Glucose (Wako, Osaka, Japan). Plasma insulin concentration was measured by an enzyme-linked immunosorbent assay (ELISA) kit specific to insulin (Morinaga Seikagaku, Yokohama, Japan). Plasma concentrations of total cholesterol, high-density lipoprotein (HDL) cholesterol, and triglyceride were measured by using cholesterol E-Wako, HDL cholesterol E-Wako, and triglyceride E-Wako (Wako), respectively.

2.3. Morris water maze test

Behavioral testing was performed with a modified version of the Morris water maze test to assess spatial navigation learning and memory retention, as previously reported

(Fitz et al., 2010), with minor modifications. Initially, animals received a habituation trial during which the animals were allowed to explore the pool of water (diameter 120 cm, height 25 cm, temperature 21±°C) without the platform present.

Visual cue phase. Following habituation, visible platform training was performed to measure motivation of the mice to find a platform, visual acuity of the mice, and the ability of mice to use local cues. Briefly, distal cues were removed from around the pool, and the platform was labeled with a flag and placed 1 cm above the surface of the water in the center of a quadrant. Mice were placed in the maze and allowed to explore the maze for 60 seconds, and if they reached the visible platform, they were allowed to remain there for 20 seconds before being returned to their cages. If they did not find the platform within 60 seconds, the experimenter led them to the platform and let them remain there for 20 seconds. Animals were trained in groups of 5, and training was completed once each animal received 6 trials. This training was performed for 1 day.

Acquisition phase. We measured the ability of mice to form a representation of the spatial relationship between a safe, but invisible (submerged 1 cm below the water level), platform (10 cm in diameter) and visual cues surrounding the maze. The platform was located in the center of 1 of the 4 quadrants, and several extramaze cues were distributed across the walls surrounding the pool. During the acquisition phase of training, each mouse received 4 daily hidden platform training trials with 10–12-minute intervals for 5 consecutive days. Animals were allowed 60 seconds to locate the platform and 20 seconds to rest on it. Mice that failed to find the platform were led there by the experimenter and allowed to rest there for 20 seconds.

Probe trial phase. Twenty-four hours after the last acquisition trial, a single 60-second probe trial was administered to assess spatial memory retention. For the probe trial, animals were returned to the pool without the platform present, and parameters were recorded to assess the ability of the mouse to remember the previous location of the platform.

Performance was recorded with an automated tracking system (TARGET series/2, Japan) during all phases of training. During the visual cue phase of training, speed and latency to the platform were used to compare the activity of the performance between each group. During the acquisition phase, acquisition time (latency to reach the platform) and path length (swum distance) were subsequently used to analyze and compare the performance between different treatment groups. The time to the platform quadrant and the number of entries into the target quadrant were recorded and analyzed during the probe trials.

2.4. Immunoblotting and filter trap assay

For immunoblotting analysis, the brain was extracted and rapidly frozen using liquid nitrogen. The brain samples from the cerebrum of the male mice were extracted in radioimmunoprecipitation assay (RIPA) buffer (50 mM Tris–HCl, 150 mM NaCl, 1% Triton X100, 1% NP-40, 0.5% deoxycholate, 0.1% SDS, pH 8.0) with protease inhibitor cocktail (Roche, Basel, Switzerland) and sufficiently homogenized on ice. Then the samples were incubated for one night at 4 °C and centrifuged at 14,000*g* for 20 minutes. The supernatants were directly used for Western blot analysis. The detailed protocol has been described previously (Maesako et al., 2011). Mouse monoclonal anti-Aβ (6E10), β-actin, and rabbit polyclonal anti-APP C-terminal antibodies were from Sigma-Aldrich (St. Louis, MO).

Filter trap assay was conducted as described previously (Kitaguchi et al., 2009). Briefly, the protein concentration of the samples in Tris-buffered saline (TBS)-extracted fraction was measured, and an equal amount of protein was subjected to vacuum filtration through a 96-well dot blot apparatus (Bio-Rad Laboratories, Hercules, CA) containing 200-nm pore-sized nitrocellulose membrane. The resultant membrane was then incubated with primary Aβ oligomer antibody (A11, Invitrogen, Carlsbad, CA; diluted 1:1000) at 4 °C overnight. The membrane was then blocked by TBS containing 4% skim milk and incubated with HRP-linked anti-mouse IgG secondary antibody (GE Healthcare, Little Chalfont, Buckinghamshire, UK; diluted 1:2000) for 1 hour. The membrane was developed using the ECL Western Blotting Analysis System (GE Healthcare). Aβ42 peptides (Bachem, Bubendorf, Switzerland) incubated for 60 minutes at 37 °C were used as a positive control (Maesako et al., 2010), and monomeric Aβ was used as a negative control.

2.5. Immunohistochemistry

The paraformaldehyde-fixed and paraffin-embedded tissue sections of male mice were incubated with anti-Aβ (6E10) antibody (1:1000). The sections were then incubated with biotinylated anti-mouse IgG antibody (1:2000; Vector Laboratories, Burlingame, CA, USA), followed by the incubation with avidin peroxidase (ABC Elite kit; 1:4000; Vector Laboratories). Subsequently, the labeling was visualized by incubation with 50 mM Tris–HCl buffer (pH 7.6) containing 0.02% 3,3-diaminobenzidine and 0.0045% hydrogen peroxide. All images were visually analyzed using a microscope, ECLIPSE 80i (Nikon Corp., Tokyo, Japan). On the other hand, for the fluorescent analysis, the tissue sections were incubated with anti-Aβ (6E10) antibody, followed by incubation with Alexa Fluor 488 anti-mouse IgG (Invitrogen). All images were visually analyzed using a laser confocal scanning microscope, FV10i-LIV (Olympus Corp., Tokyo, Japan). The Aβ immunoreactivity was quantified with Image J. For each animal, the sections were captured in the cortex and the hippocampus. Captured im-

ages then were imported into Image J, and an intensity threshold level was set that allowed for discrimination between plaque and background labeling. The total number of Aβ plaque-associated pixels (6E10 antibody-positive pixels) was calculated in each section, and then the Aβ load was calculated.

2.6. Measurement of Aβ by ELISA

The levels of Aβ40, Aβ42, or Aβ oligomers were measured by ELISA kits specific to Aβ40, Aβ42, or Aβ oligomers (82E1-specific) (Immuno-Biological Laboratories Co., Ltd., Gumma, Japan), according to the manufacturer's instructions. We used a standard format for measuring monomeric Aβ species with the use of C-terminal capturing antibodies and N-terminal or midregion detecting antibodies. On the other hand, to detect Aβ oligomer species, the same N-terminal antibody, 82E1 (to Aβ residues 1–16; Immuno-Biological Laboratories, Inc), was used for both capture and detection. To prepare the samples, the brain samples from the cerebrum of the male mice were homogenized with TBS. The homogenate was centrifuged at 100,000*g* for 1 hour, and the supernatant was collected as the TBS-extracted fraction. Seventy percent formic acid (FA) was added to the pellet, which was homogenized again. The homogenate was incubated for 1 hour at 4 °C and then centrifuged at 100,000*g* for 1 hour at 4 °C. The resultant supernatant was collected as the FA-extracted fraction, which was neutralized with a 20-fold volume of 1 M Tris buffer (pH 11.0).

2.7. Statistical analysis

All values are given in means ± SE. Comparisons were performed using an unpaired Student's *t*-test. For comparison of multiparametric analysis, one-way factorial ANOVA, followed by the post hoc analysis by Fisher's PLSD, was used. Statistical significance of differences between mean scores during acquisition phase of training in the Morris water maze test was assessed with two-way repeated-measures ANOVA (general linear model/RM-ANOVA) and Fisher's post hoc analysis for multiple comparisons. A $p < 0.05$ was considered to indicate a significant difference.

3. Results

3.1. Environmental enrichment ameliorated HFD-induced metabolic dysfunctions

Recent literature has demonstrated that HFD disrupts the metabolic conditions of APP Tg mice (Ho et al., 2004). To determine the effect of EE on HFD-induced metabolic dysfunctions, the cage of APP-HFD mice was changed into a larger one with a running wheel and objects like stands and toys. The mice were then fed with HFD for 10 weeks (Fig. 1). T2DM is characterized by obesity, glucose intolerance, and hyperinsulinemia (Defronzo, 2009). According to our metabolic analysis using weekly monitoring of body weight, an IGTT, and the ELISA of serum insulin, obesity, glucose intolerance, and hyperinsulinemia were observed in the APP-HFD mice. Thus, we conclude that the APP-HFD mice, which we generated, exhibited severe T2DM conditions.

Although the APP-HFD mice gained significantly more body weight than the control APP mice (standard diet), the APP-HFD with EE (APP-HFD + EE) mice gained less body weight than the APP-HFD mice after the transfer to the EE setting (Fig. 2A). Despite being fed with HFD, the APP-HFD + EE mice maintained an even body weight for 10 weeks. Weekly monitoring of food intake showed that the amount of food intake by the APP-HFD + EE mice was larger than that of the APP-HFD mice (supplemental Fig. 1), which indicated that the EE-mediated attenuation of body weight was not caused by the reduction of food intake. Moreover, we monitored the number of running wheel rotation and estimated that the APP-HFD + EE mice ran 1040 ± 49 m per day in the EE setting. The fasting glucose level of the APP-HFD mice was increased, compared with that of the control APP mice, whereas that of the APP-HFD + EE mice was significantly decreased, compared with that of the APP-HFD mice (Fig. 2B). Further, the IGTT results indicated that the impaired glucose tolerance response of the APP-HFD mice was improved in the APP-HFD + EE group (Fig. 2C). To examine whether EE could reverse or prevent glucose tolerance abnormality, we conducted IGTT at the time of the switch from the standard environment to the enriched one (10 weeks after HFD introduction). The fasting glucose level and glucose tolerance of APP-HFD + EE mice were better than those of the APP mice at the time of the switch (supplemental Fig. 2). Therefore, EE could reverse glucose tolerance abnormality. The ELISA results indicated that the level of plasma insulin was significantly increased in the APP-HFD mice. However, in contrast with the glucose level, the plasma insulin level tended to decrease to some extent, but was not significantly different between the APP-HFD and APP-HFD + EE mice (Fig. 2D).

Next, we conducted plasma lipid analyses. The level of plasma total cholesterol in the APP-HFD mice was significantly increased compared with that of the control APP mice. On the other hand, the total cholesterol level of the APP-HFD + EE mice was not different from that of the APP-HFD mice (Fig. 3A). Similarly, the level of plasma HDL cholesterol in APP-HFD mice was significantly increased compared with that in the control APP mice. The plasma HDL level of the APP-HFD + EE mice was comparable with that of the APP-HFD mice (Fig. 3B). On the contrary, the level of plasma triglycerides was not different among the 3 conditions (Fig. 3C). Taken together, these results indicated that HFD disrupted the metabolic conditions including body weight, glucose tolerance, plasma in-

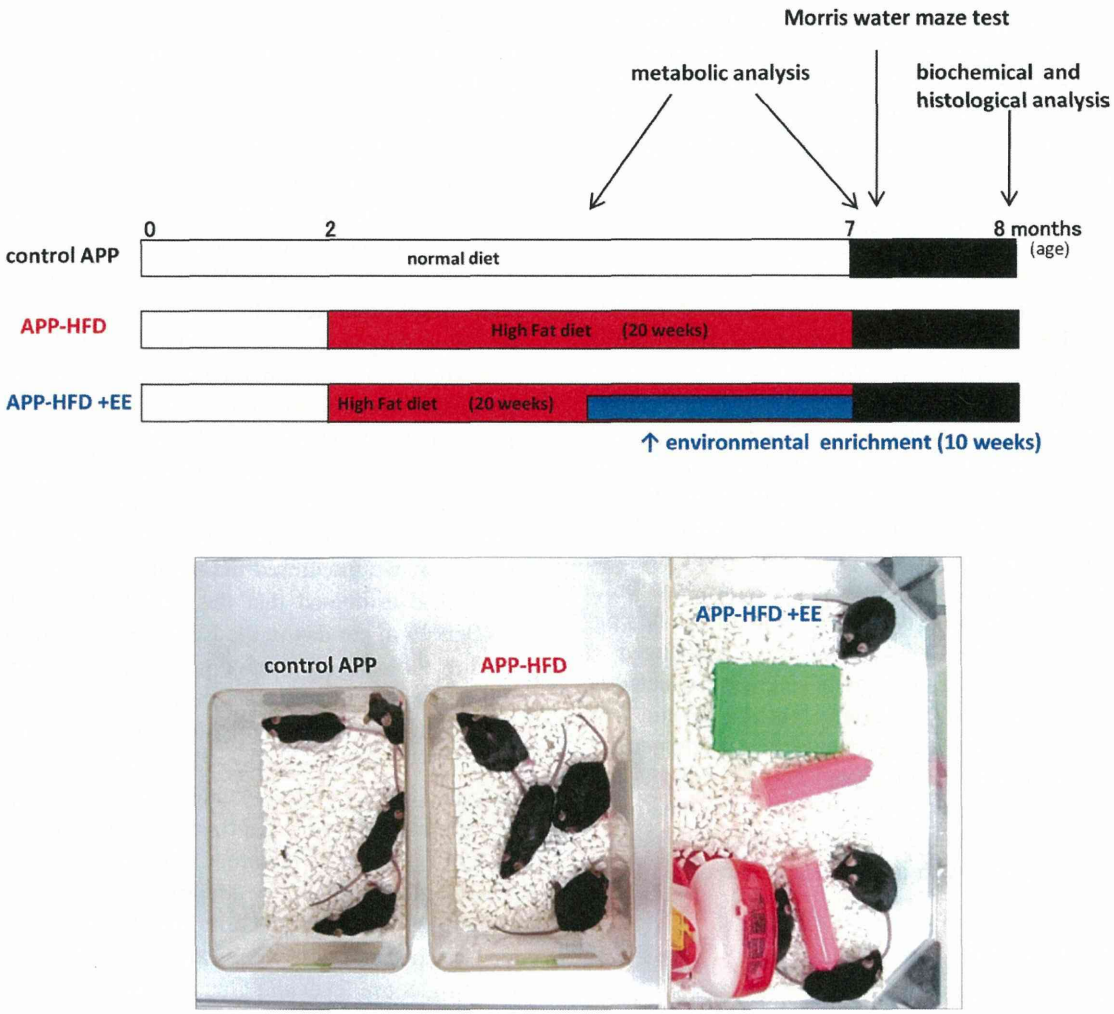

Fig. 1. Schematic presentation of our experimental design. APP *Swe/Ind* mice were maintained with standard diet in the standard laboratory cages until 2–3 months of age. Then, age- and sex-matched mice were separated into 3 groups. In the control group, the mice were induced with standard diet in the standard laboratory cages for 20 weeks (control APP mice) (top row, n = 9). In the high-fat diet (HFD)-induced group, the mice were fed with HFD in the standard laboratory cages for 20 weeks (APP-HFD mice) (middle row, n = 10). In the HFD with environmental enrichment (EE)-induced group, the mice spent 10 weeks in the standard laboratory cages, then spent 10 weeks in the enrichment cages with HFD (APP-HFD + EE mice) (bottom row, n = 8). After 20 weeks, metabolic conditions of these mice were analyzed, followed by ethological, histochemical, and biochemical analyses targeting AD pathophysiology. For interpretation of the references to color in this figure legend, the reader is referred to the Web version of this article.

sulin, and cholesterols of APP Tg mice, among which EE ameliorated body weight and glucose tolerance.

3.2. Environmental enrichment improved HFD-induced memory deficit

Recent literature also demonstrated that HFD leads to the worsening of memory deficit in APP Tg mice (Ho et al., 2004). To determine the effect of EE on HFD-induced memory deficit, we conducted the Morris water maze test. In our study, we analyzed 7- to 8-month-old APP Tg mice because they present with visible Aβ plaques and cognitive impairment sufficient for quantitative evaluations (Mucke et al., 2000). Neither HFD nor HFD + EE increased mortality of the mice, nor did they affect the motivation during the visual cue phase of the test (data not shown). In addition, neither HFD nor HFD + EE affected the locomotor activity of the mice, as exemplified by swimming speed (supplemental Fig. 3). During the acquisition phase, the control APP mice showed a daily improvement in their performance, such as acquisition time (Fig. 4A) and path length to the platform (Fig. 4B), whereas the APP-HFD mice did not show any improvement. On the other hand, the APP-HFD + EE mice showed better performance than the APP-HFD mice did (Fig. 4A, B). Moreover, the probe trial demonstrated that the APP-HFD mice took a longer time to get to the platform quadrant (Fig. 4C) and failed to cross the previous location of the platform (Fig. 4D), compared with control mice. Once again, the APP-HFD + EE mice showed better performance than the APP-HFD mice in this probe trial phase as well (Fig. 4C, D). From these

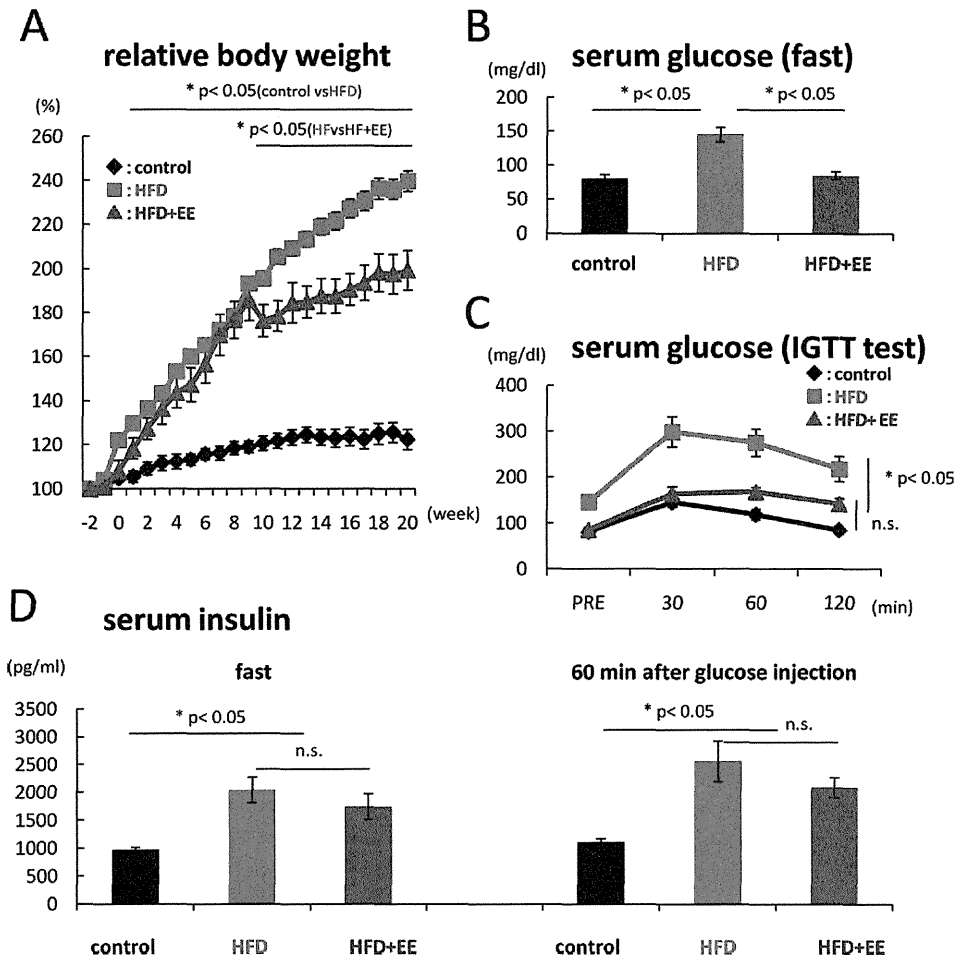

Fig. 2. Environmental enrichment ameliorated HFD-induced diabetic conditions. (A) Relative body weight changes over 20 weeks. The body weight of 2 weeks before each diet was regarded as the baseline (100%). The body weight of APP-HFD mice was significantly increased compared with that of control APP mice ($F(2,528) = 136.81$, $p < 0.05$). On the other hand, that of APP-HFD + EE mice was significantly decreased compared with that of APP-HFD mice ($p < 0.05$). (B) Fasting glucose levels. The fasting glucose level of APP-HFD mice was significantly increased compared with that of control APP mice ($F(2,24) = 19.38$, $p = 0.02$). On the other hand, the fasting glucose level of APP-HFD + EE mice was significantly decreased compared with that of APP-HFD mice ($p = 0.03$). (C) Blood glucose levels during glucose tolerance test after an intraperitoneal injection of glucose (2 g/kg body weight). APP-HFD mice showed impaired glucose tolerance compared with control mice ($F(2,72) = 35.00$, $p < 0.05$). On the other hand, APP-HFD + EE had ameliorated HFD-induced glucose intolerance ($p < 0.05$). (D) Serum insulin levels during fasting or 60 min after glucose injection. At both time points, the serum insulin level of APP-HFD mice was significantly increased compared with that of control APP mice ($F(2,24) = 8.08$, $p = 0.003$). The serum insulin level of APP-HFD + EE mice was not significantly decreased compared with that of APP-HFD mice (n.s., $p = 0.27$). n.s. indicated not significantly. For interpretation of the references to color in this figure legend, the reader is referred to the Web version of this article.

results, we concluded that EE ameliorated HFD-induced memory dysfunction, despite continuing HFD in the AD model mice.

To determine whether these events were attributable to metabolic consequences of the diet or to an interaction between the diet and neuropathology in AD model mice, wild-type (WT) mice were tested for learning ability using the Morris water maze test. Metabolic analyses indicated that WT mice also exhibited T2DM conditions (supplemental Fig. 4A, B). After the 4th day, in the acquisition phase of Morris water maze test, acquisition time of the HFD-induced WT (WT-HFD) mice was not different from that of the control WT or the WT-HFD + EE mice, although that of the WT-HFD mice was longer than that of the control WT and the WT-HFD + EE mice from the 1st to 3rd day (supplemental Fig. 4C). This tendency was different from the case of the APP mice because APP-HFD mice consistently took longer time to get to the platform quadrant in the acquisition phase (Fig. 4A). These results suggested that memory dysfunction could be attributable to an interaction between the diet and neuropathology in the AD model mice.

3.3. HFD-induced Aβ deposition was ameliorated in environmental enrichment condition

HFD is reported to lead to Aβ accumulation in the brain of APP Tg mice (Ho et al., 2004). We considered the

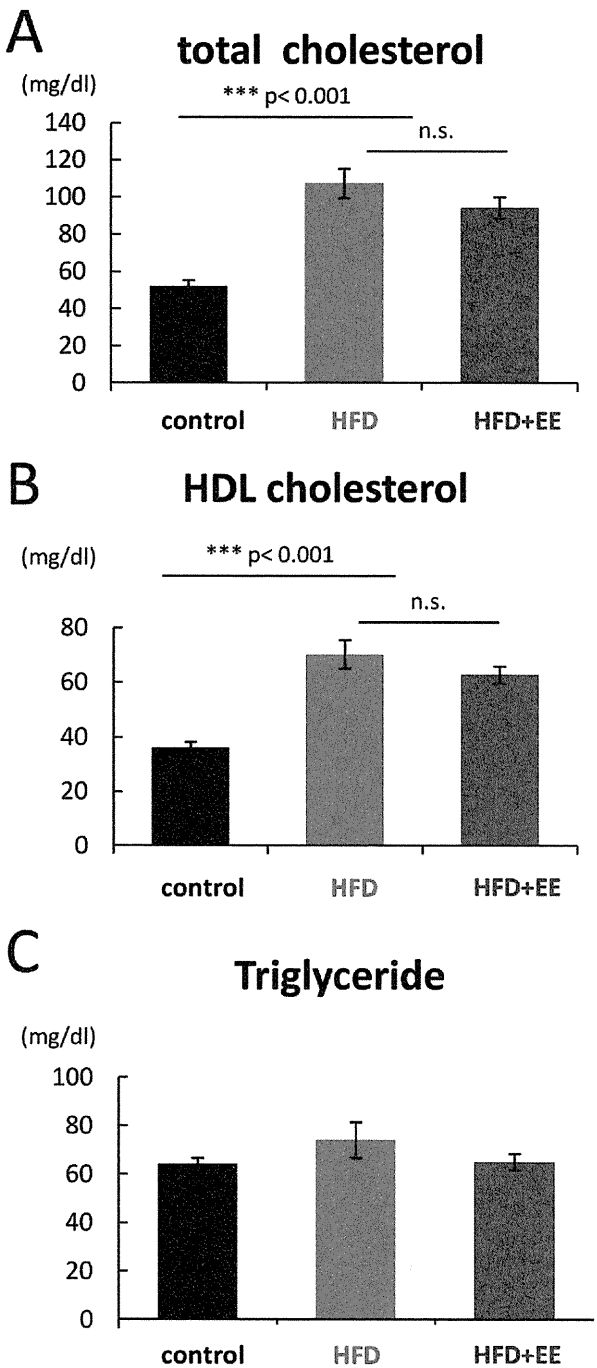

Fig. 3. Environmental enrichment could not ameliorate HFD-induced lipid dysfunction. (A) Plasma total cholesterol levels. The total cholesterol level of APP-HFD mice was significantly increased compared with that of control APP mice ($F(2,24) = 24.28$, $p = 0.0003$). That of APP-HFD + EE mice was not significantly decreased compared with that of APP-HFD mice (n.s., $p = 0.14$). n.s. indicated not significantly. (B) Plasma HDL cholesterol levels. The HDL cholesterol level of APP-HFD mice was significantly increased compared with that of control APP mice ($F(2,24) = 17.37$, $p = 0.0003$). The HDL cholesterol level of APP-HFD + EE mice was not significantly decreased compared with that of APP-HFD mice (n.s., $p = 0.17$). n.s. indicated not significantly. (C) Plasma triglyceride levels. There was no difference among control, APP-HFD, and APP-HFD + EE mice ($F(2,24) = 1.33$, n.s.). For interpretation of the references to color in this figure legend, the reader is referred to the Web version of this article.

possibility that the memory impairment in APP-HFD mice was due to ample Aβ deposition and wanted to see the effect of environmental change on HFD-induced Aβ accumulation. Therefore, we conducted immunohistochemical analysis using anti-Aβ (6E10) antibody to quantitatively examine Aβ deposition. As seen in Fig. 5A–C, Aβ deposition in the hippocampus was aggravated in the APP-HFD mice, whereas EE introduction resulted in a marked reduction of HFD-induced Aβ deposition in the APP-HFD + EE mice.

We next quantified Aβ contents in the TBS-soluble and insoluble (FA soluble) fractions using ELISA. In the TBS-soluble fraction, the levels of Aβ40, Aβ42, and total Aβ in the APP-HFD mice were comparable with that in the control APP mice. However, the levels of Aβ40 and total Aβ in the APP-HFD + EE mice were significantly decreased compared with that in the APP-HFD mice (Fig. 5D–F). On the other hand, in FA fraction, the level of Aβ40 in the APP-HFD mice was significantly increased compared with that in the control APP mice. However, the levels of Aβ 40 in the APP-HFD + EE mice were significantly decreased compared with that in the APP-HFD mice (supplemental Fig. 5A). A similar tendency was shown in the case of Aβ42 and total Aβ amount in FA fraction, although there was no statistical significance (supplemental Fig. 5B, C). Based on these histochemical and biochemical analyses, we concluded that EE ameliorated HFD-induced Aβ accumulation in the brain.

Recent reports suggest that the level of soluble Aβ oligomers correlate with memory deficits in APP Tg mice (Hartley et al., 1999; Lesné et al., 2006; Shankar et al., 2009; Walsh et al., 2002). To determine a correlation between Aβ oligomers and memory impairment in standard housing APP-HFD mice and APP-HFD + EE mice, we performed the ELISA analysis using Aβ oligomer-specific ELISA kit (Xia et al., 2009). The level of TBS-soluble Aβ oligomers in the APP-HFD mice was significantly increased compared with that in the control APP mice. This result was consistent with that of the test for memory assessment described previously. Remarkably, the levels of Aβ oligomers in the APP-HFD + EE mice were significantly decreased compared with that in the APP-HFD mice (Fig. 5G). In addition, we confirmed this result through filter trap assay, using anti-Aβ oligomer antibody (supplemental Fig. 6). Thus, at least in HFD-induced conditions, EE appears to play a significant role in modulating the level of Aβ oligomers.

3.4. Alteration of HFD-induced APP processing by environmental enrichment

To elucidate the mechanism of how EE ameliorated HFD-induced Aβ accumulation, we analyzed the APP processing through detecting APP C-terminal fragments (CTFs: CTFα, β) through immunoblotting assay. The α- and β-secretases are known to cleave APP at the extramembrane domain and produce APP-CTFα and CTFβ, respectively. γ-Secretase cleaves APP-CTFα and CTFβ at the intramembrane domain, producing p3 and Aβ, respectively. As shown in the top row of Fig. 6A, the level of full-length APP was not different among the

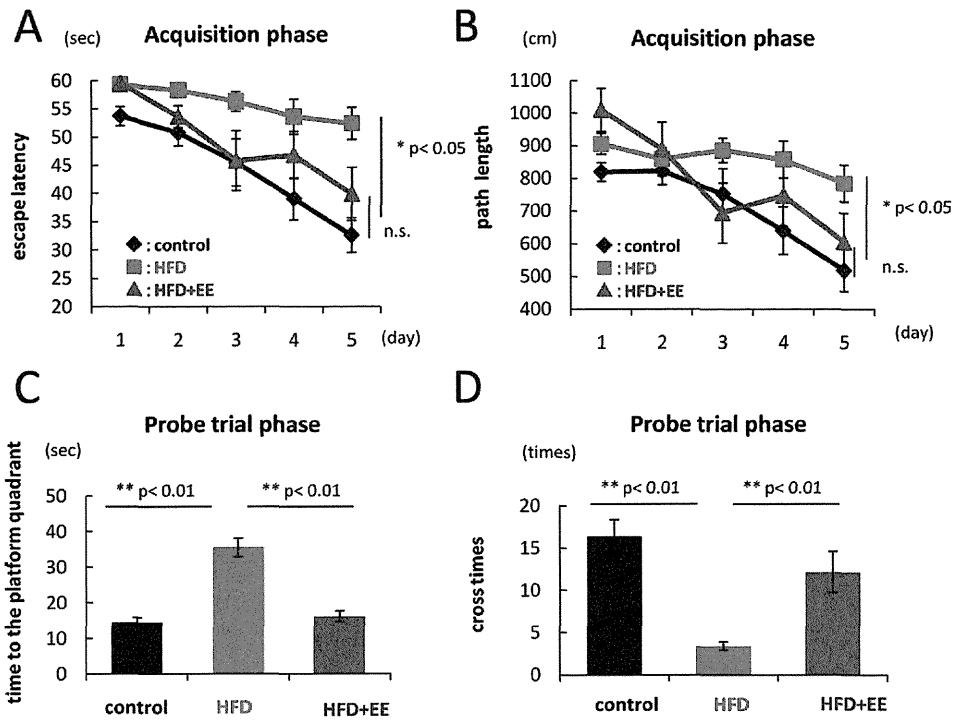

Fig. 4. Environmental enrichment ameliorated HFD-induced memory deficit. (A) Escape latency in the acquisition phase. APP-HFD mice significantly took longer time to the platform compared with control APP mice ($F(2,96) = 17.33$, $p = 0.012$). On the other hand, APP-HFD + EE mice took less time than APP-HFD mice ($p = 0.34$). (B) Swimming length in the acquisition phase. APP-HFD mice swam significantly longer than control APP mice ($F(2,96) = 11.92$, $p = 0.025$). On the other hand, APP-HFD + EE mice swam shorter than APP-HFD mice ($p = 0.37$). (C) The time to the target quadrant in the probe trial phase. APP-HFD mice significantly took longer time to the platform quadrant compared with control APP mice ($F(2,24) = 33.02$, $p = 0.002$). On the other hand, APP-HFD + EE mice took less time than APP-HFD mice ($p = 0.002$). (D) The number of entries into the target quadrant in the probe trial phase. APP-HFD mice were significantly impaired in the number of times they crossed the platform compared with control APP mice ($F(2,24) = 15.75$, $p = 0.0014$). On the other hand, APP-HFD + EE mice increased the number of times they crossed the platform compared with APP-HFD mice ($p = 0.003$). For interpretation of the references to color in this figure legend, the reader is referred to the Web version of this article.

control, APP-HFD, and APP-HFD + EE mice (Fig. 6B). In this experiment, we used anti-APP C-terminal antibody to detect both APP-CTFα and CTFβ. Notably, APP CTFs were more accumulated in the brains of the APP-HFD mice than those of the control APP mice. However, the level of APP CTFs in the APP-HFD + EE mice was significantly decreased compared with that in the APP-HFD mice in standard housing (Fig. 6C). Next, we examined the amount of APP-CTFβ by anti-Aβ (6E10) antibody, which detects 1–17 amino acid residues of Aβ. The analysis using 6E10 antibody showed that the level of APP-CTFβ in the APP-HFD mice was higher than that in the control APP mice, suggesting that the level of APP-CTFβ in the APP-HFD + EE mice was significantly decreased compared with that in the APP-HFD mice (Fig. 6D).

4. Discussion

HFD is prevalent in modern society, and HFD-induced metabolic condition is becoming a worldwide issue because it leads to obesity, T2DM, and hypercholesterolemia. More importantly, recent studies have shown that diet and nutrition have been recognized as important epigenetic factors for the development of sporadic AD (Panza et al., 2006; Scarmeas et al., 2007; Solfrizzi et al., 2003). We and others have previously proposed the causal molecular link between T2DM and AD (Maesako et al., 2010, 2011; Qiu and Folstein, 2006). However, the effective prevention for AD has not been fully investigated yet. A recent report by McClean et al. showed compelling evidence that the diabetes drug liraglutide prevents neuronal degeneration in a mouse model of AD (McClean et al., 2011), which suggests that there should be a clinical association of diabetic change with a higher risk of neuronal loss. This further led us to consider a development of an effective prevention in the early phase of AD. To address this issue, we established the AD model mice with diabetic conditions in the present study, by HFD feeding in APP Tg mice.

To search for an effective intervention, we chose a paradigm of EE and examined the effect of EE on both the metabolic conditions and the AD pathology of the mice (Fig. 1). A recent retrospective case-control study demonstrated that AD patients were less active (both intellectually and physically) in midlife and that inactivity was associated with a 2.5-fold higher risk of developing AD (Friedland et al., 2001). Similarly, a prospective study revealed that phys-

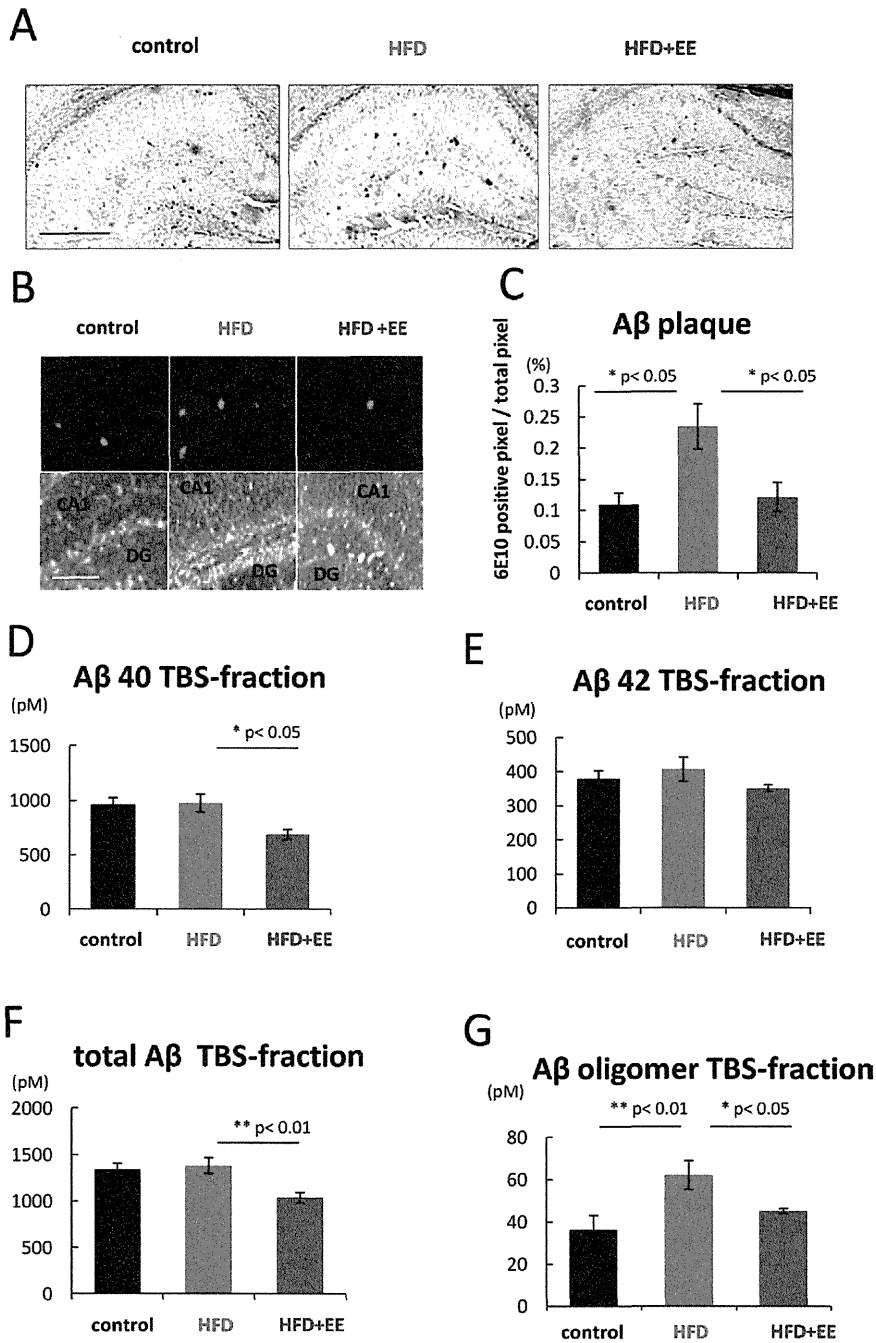

Fig. 5. Environmental enrichment ameliorated HFD-induced Aβ accumulation. (A) Immunohistochemical analysis using anti-Aβ (6E10) antibody. Representative images of Aβ-immunostained hippocampus sections from control APP, APP-HFD-, and APP-HFD + EE-induced mice, respectively. Scale bar, 2 mm. (B) High-magnification images of the hippocampus including CA1 and dentate gyrus (DG) regions by immunostained analysis using anti-Aβ (6E10) antibody and Alexa Fluor 488 2nd antibody. The immunostained signal was much enhanced in APP-HFD mice compared with that in control APP and APP-HFD + EE mice. Scale bar, 0.5 mm. (C) Cerebral Aβ loads determined by immunohistochemical and morphometric analyses. The cerebral Aβ deposition was significantly increased in APP-HFD mice compared with that in control APP mice ($F(2,10) = 5.62$, $p = 0.012$). On the other hand, that in APP-HFD + EE mice was significantly decreased compared with that in APP-HFD mice ($p = 0.023$). (D) ELISA of Aβ40 in TBS-soluble fraction. The level of TBS-soluble Aβ40 in APP-HFD mice was the same as that in control APP mice. On the other hand, that in APP-HFD + EE was significantly decreased compared with that in APP-HFD mice ($F(2,10) = 5.16$, $p = 0.015$). (E) ELISA of Aβ42 in TBS-soluble fraction. There was no statistical significance among control APP, APP-HFD-, and APP-HFD + EE-induced mice ($F(2,10) = 1.05$, n.s.). (F) ELISA of total Aβ (Aβ40 + Aβ42) in TBS-soluble fraction. The level of TBS-soluble total Aβ in APP-HFD mice was the same as that in control APP mice. On the other hand, that in APP-HFD + EE was significantly decreased compared with that in APP-HFD mice ($F(2,10) = 6.35$, $p = 0.037$). (G) ELISA of Aβ oligomer in TBS-soluble fraction. The cerebral Aβ oligomer was significantly increased in APP-HFD mice compared with that in control APP mice ($F(2,10) = 5.19$, $p = 0.01$). On the other hand, that in APP-HFD + EE was significantly decreased compared with that in APP-HFD mice ($p = 0.049$). For interpretation of the references to color in this figure legend, the reader is referred to the Web version of this article.

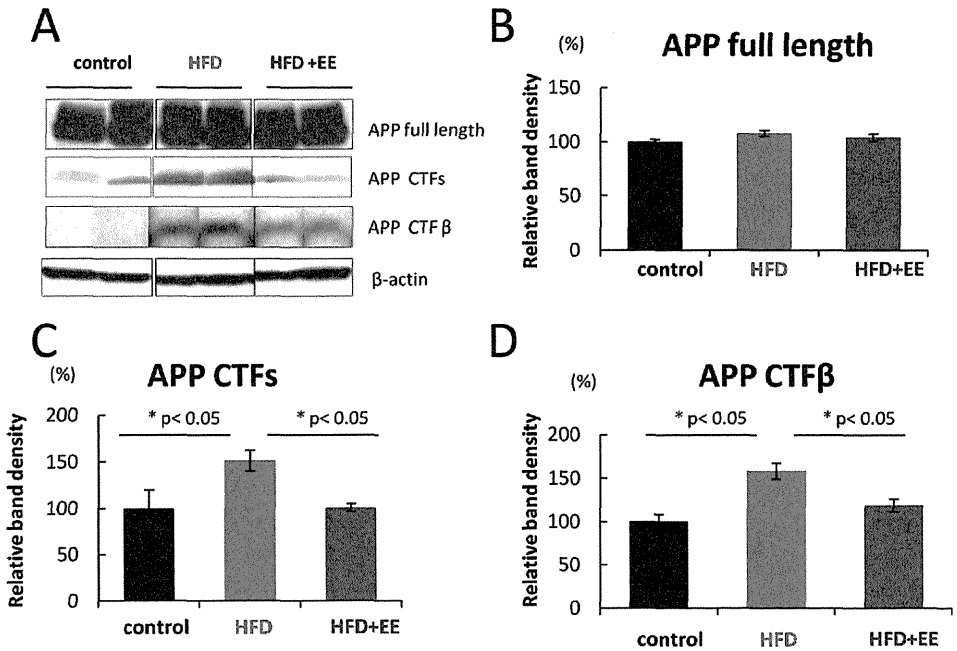

Fig. 6. Environmental enrichment reduced APP CTFβ accumulation. (A) Immunoblotting analysis of APP full length, APP CTFs (CTFα, β), and APP CTFβ. APP full length and APP CTFs were detected by anti-APP C-terminus antibody. APP CTFβ was detected by anti-Aβ (6E10) antibody. Two different samples from each group were shown. β-Actin was detected as loading control. (B) Statistical analysis of APP full length. The band of APP full length was normalized by that of β-actin. The band density of the control was regarded as 100% and that of other groups was relatively indicated. There was no statistical significance among control APP, APP-HFD, and APP-HFD + EE mice ($F(2,10) = 2.36$, n.s.). (C) Statistical analysis of APP CTFs. The band of APP CTFs was normalized by that of APP full length. The band density of APP CTFs in APP-HFD mice was increased compared with that in control APP mice ($F(2,10) = 4.73$, $p = 0.013$). On the other hand, that in APP-HFD + EE mice was significantly decreased compared with that in APP-HFD mice ($p = 0.015$). (D) Statistical analysis of APP CTFβ. The band of APP CTFβ was normalized by that of APP full length. The band density of APP CTFβ in APP-HFD mice was increased compared with that in control APP mice ($F(2,10) = 5.67$, $p = 0.011$). On the other hand, that in APP-HFD + EE mice was significantly decreased compared with that in APP-HFD mice ($p = 0.032$). For interpretation of the references to color in this figure legend, the reader is referred to the Web version of this article.

ical activity was protective against the development of cognitive impairment in AD and that the highest-activity group showed the incidence of AD lowered by 60% (Laurin et al., 2001). Because EE is regarded as a useful tool for exercise in mice, we chose this paradigm in the present study to see the impact of exercise on AD pathophysiology. Importantly, Adlard et al. have demonstrated that voluntary exercise shows beneficial effects on a Tg mice model of AD (Adlard et al., 2005). Because the EE condition contains physical and intellectual stimulation, the extent to which intellectual stimulation contributes to the positive outcome still remains controversial. Faherty et al. suggested that EE is more effective for facilitating neural changes than exercise alone (Faherty et al., 2003), whereas Lambert et al. suggested that exercise, but not cognitive stimulation, improves spatial memory (Lambert et al., 2005). In the setting of the present study, metabolic conditions of the APP-HFD + EE mice were clearly ameliorated compared with those of the APP-HFD mice. Moreover, cognitive stimulation of our setting was smaller than that in previous reports because we wanted to focus on the effect of exercise on APP-HFD mice. Therefore, we speculated that physical stimulation might play a more important role in our study. The purpose of this experiment was to obtain a deep insight into developing strategies for the prevention of AD; therefore, EE was started at the age before the appearance of visible Aβ plaques in the brain of APP *Swe/Ind* mice.

Although previous reports examined the effect of EE on AD model mice (Cotel et al., 2012; Hu et al., 2010; Jankowsky et al., 2003, 2005; Lazarov et al., 2005), the effect of EE on AD mice with diabetic conditions had not yet been examined. Notably, our results indicated that EE ameliorated HFD-induced memory deficit, despite continuing high-fat feeding (Fig. 4). EE is known to enhance hippocampal neurogenesis and result in increased numbers of synapses per neuron (Hu et al., 2010). We assumed that EE might have improved cognitive dysfunctions of the mice through strengthening of the synaptic activity of the mice. Further, our results demonstrated that EE decreased oligomers and fibrillar Aβ, indicating that EE also ameliorated HFD-induced Aβ accumulation (Fig. 5). An increasing number of reports have suggested that the level of soluble Aβ oligomers correlates with memory deficits due to their synaptotoxicity (Hartley et al., 1999; Jin et al., 2011; Lesné et al., 2006; Shankar et al., 2009; Walsh et al., 2002). Therefore, we hypothesized that EE also might have im-

proved memory deficit of the mice through the decrease of soluble Aβ oligomers, followed by the improvement of Aβ plaque depositions. Notably, Cotel et al. have reported that EE failed to rescue working memory deficits and neuronal loss in APP/PS1 knock-in (KI) mice (Cotel et al., 2012). Their result is different from ours in that enriched housing did not show any beneficial effects in terms of working memory and amyloid burden. Our result was obtained from high-fat feeding of APP Tg mice, whereas Cotel et al. used conventional diet for APP/PS1 KI mice; however, housing conditions seem similar. We suppose that the combination of physical activity and cognitive stimulus in EE condition may be more beneficial in the reversal of cognitive decline and Aβ load, which was caused by metabolic dysfunctions due to high-fat feeding.

To clarify the effect of EE on HFD-induced AD pathology, we first investigated the mechanisms of how HFD aggravated Aβ depositions. Recent literature has suggested that HFD downregulates the activity of insulin-degrading enzyme (IDE), one of the Aβ-degrading enzymes (Ho et al., 2004). In addition, we demonstrated that HFD increased the level of APP CTFβ without a change in full-length APP levels (Fig. 6). Unexpectedly, we could not detect the difference of beta-site APP cleaving enzyme 1 (BACE1)/β-secretase level among control APP, APP-HFD, and APP-HFD + EE mice's brains (supplemental Fig. 7A, B). Although emerging evidence has consistently detected significant increases in β-secretase enzyme activity in the sporadic AD brains, the BACE1 enzyme activity in AD is not necessarily reflected by its protein levels (Stockley and O'Neill, 2008), presumably because BACE1 enzyme activity might be regulated by other factors such as trafficking, and subcellular and membrane microdomain localization. Moreover, recent literature has demonstrated that BACE1 enzyme activity is modulated by sphingosine-1-phosphate (S1P), a pluripotent lipophilic mediator (Takasugi et al., 2011), suggesting that BACE1-interacting proteins can also control its activity. We compared the BACE1-interacting proteins of the APP-HFD mice brain samples with that of the control APP samples by immunoprecipitation assay using BACE1 antibody and determined the different profiles in interacting proteins between them (unpublished observation). We speculate that HFD might have changed the interacting state of these proteins with BACE1, without changing the BACE1 protein level. Consequently, we conclude that HFD could have aggravated Aβ accumulation via several pathways, including the activation of BACE1/β-secretase enzyme and the inhibition of Aβ degradation.

Next, to reveal the mechanism of beneficial effect of EE, we used ELISA experiments. The ELISA results in TBS-soluble fraction indicated that HFD might not simply increase the production of Aβ, but that HFD affects the aggregation and deposition of Aβ (Fig. 5D–F). On the other hand, considering that EE decreased the level of APP CTFβ (Fig. 6), we assume that EE could have inhibited HFD-induced BACE1/β-secretase upregulation. We speculate that EE could also have changed the state of interacting proteins with BACE1. However, EE also might have improved Aβ accumulation via the upregulation of Aβ clearance because EE activates neprilysin, one of the Aβ-degrading enzymes (Lazarov et al., 2005). Interestingly, our metabolic analyses suggested that EE did not affect either HFD-induced hyperinsulinemia or hypercholesterolemia, but improved body weight as well as glucose tolerance (Figs. 2 and 3), indicating that EE might have ameliorated HFD-induced Aβ accumulation through the improvements in obesity and glucose tolerance. According to a recent review by Misra, the EE-mediated improvement of glucose tolerance via insulin-independent pathway may be caused by the role of adenosine monophosphate (AMP)-activated protein kinase (AMPK) because it is considered a master switch to regulate glucose level without an effect on insulin in exercise-related effects (Misra, 2008). To develop an effective intervention, it is important to elucidate the relationship between obesity and glucose intolerance and HFD-induced Aβ accumulation as well as memory deficit.

In conclusion, we provide convincing evidence that EE ameliorated HFD-induced metabolic dysfunctions, Aβ deposition, and memory deficit. We showed that EE improved metabolic conditions like obesity and glucose intolerance in APP-HFD mice without rectifying the level of serum insulin. Our result is clinically intriguing in that a rather mild intervention like EE for only 10 weeks prevented further HFD-induced cognitive decline in the AD mouse model. However, the detailed mechanism of how EE ameliorated HFD-induced Aβ deposition and memory deficit was not clarified in the present study. Although the exact pathogenesis of sporadic AD remains still largely unknown, our results clearly indicate that the intervention for the metabolic condition could be the most effective and practicable way to prevent AD in T2DM patients. Considering that the beneficial effect was obtained even with the continuation of HFD, the detailed mechanism of continuous exercise and its practical application to AD patients should be further verified in future studies.

Disclosure statement

All authors do not have any actual or potential conflicts of interest including any financial, personal, or other relationships with other people or organizations within three years of beginning the work submitted that could inappropriately influence (bias) our work.

Any author's institutions do not have contracts relating to this research through which it or any other organization may stand to gain financially now or in the future.

We verify that the data contained in the manuscript being submitted have not been previously published, have not been submitted elsewhere, and will not be submitted elsewhere while under consideration at *Neurobiology of Aging*.

We verify that appropriate approval and procedures were used concerning animal materials.

We verify that all authors have reviewed the contents of the manuscript being submitted, approved of its contents, and validated the accuracy of the data.

Acknowledgements

We would like to give our thanks to Dr. S. Oka (Kyoto University, Kyoto, Japan), Mr. J. Morise (Kyoto University, Kyoto, Japan), Dr. Y. Kitamura (Kyoto Pharmaceutical University, Kyoto, Japan), and Dr. K. Takata (Kyoto Pharmaceutical University, Kyoto, Japan) for technical assistance of the brain sample preparation. We would like to give our thanks to Dr. K. Saito (Kyoto University, Kyoto, Japan) for kind support of the Morris water maze test. We greatly appreciate the advice for metabolic analysis to Dr. M. Okuda (PHARMAEIGHT. Kyoto, Japan). We would like to give our thanks to Dr. Y. Tashiro (Kyoto University, Kyoto, Japan) for kind discussion. The work was financially supported by Grant-in-Aid from the Ministry of Education, Culture, Sports, Science and Technology (20300124), the Research Grant from Takeda Science Foundation, the Research Grant from the Kanae Foundation for the Promotion of Medical Science, and the Research Grant from the Nakatomi Foundation.

Appendix

Supplementary data associated with this article can be found, in the online version, at doi: 10.1016/j.neurobiolaging.2011.10.028.

References

Adlard, P.A., Perreau, V.M., Pop, V., Cotman, C.W., 2005. Voluntary exercise decreases amyloid load in a transgenic model of Alzheimer's disease. J. Neurosci. 25, 4217–4221.

Bertram, L., Tanzi, R.E., 2008. Thirty years of Alzheimer's disease genetics: the implications of systematic meta-analyses. Nat. Rev. Neurosci. 9, 768–778.

Biessels, G.J., Staekenborg, S., Brunner, E., Brayne, C., Scheltens, P., 2006. Risk of dementia in diabetes mellitus: a systematic review. Lancet Neurol. 5, 64–74 [DOI: 10.1016/S1474-4422(05)70284-2].

Cao, D., Lu, H., Lewis, T.L., Li, L., 2007. Intake of sucrose-sweetened water induces insulin resistance and exacerbates memory deficits and amyloidosis in a transgenic mouse model of Alzheimer disease. J. Biol. Chem. 282, 36275–36282.

Cotel, M.C., Jawhar, S., Christensen, D.Z., Bayer, T.A., Wirths, O., 2012. Environmental enrichment fails to rescue working memory deficits, neuron loss, and neurogenesis in APP/PS1KI mice. Neurobiol. Aging. 33, 96–107.

Cotman, C.W., Berchtold, N.C., 2007. Physical activity and the maintenance of cognition: learning from animal models. Alzheimers Dement. 3, S30–S37.

De Strooper, B., Saftig, P., Craessaerts, K., Vanderstichele, H., Guhde, G., Annaert, W., Von Figura, K., Van Leuven, F., 1998. Deficiency of presenilin-1 inhibits the normal cleavage of amyloid precursor protein. Nature 391, 387–390.

Defronzo, R.A., 2009. Banting lecture. From the triumvirate to the ominous octet: a new paradigm for the treatment of type 2 diabetes mellitus. Diabetes 58, 773–795.

Faherty, C.J., Kerley, D., Smeyne, R.J., 2003. A Golgi-Cox morphological analysis of neuronal changes induced by environmental enrichment. Brain Res. Dev. Brain Res. 141, 55–61.

Finder, V.H., 2010. Alzheimer's disease: a general introduction and pathomechanism. J. Alzheimers Dis. 22 (suppl 3), 5–19.

Fitz, N.F., Cronican, A., Pham, T., Fogg, A., Fauq, A.H., Chapman, R., Lefterov, I., Koldamova, R., 2010. Liver X receptor agonist treatment ameliorates amyloid pathology and memory deficits caused by high-fat diet in APP23 mice. J. Neurosci. 30, 6862–6872.

Friedland, R.P., Fritsch, T., Smyth, K.A., Koss, E., Lerner, A.J., Chen, C.H., Petot, G.J., Debanne, S.M., 2001. Patients with Alzheimer's disease have reduced activities in midlife compared with healthy control-group members. Proc. Natl. Acad. Sci. U. S. A. 98, 3440–3445.

Hartley, D.M., Walsh, D.M., Ye, C.P., Diehl, T., Vasquez, S., Vassilev, P.M., Teplow, D.B., Selkoe, D.J., 1999. Protofibrillar intermediates of amyloid beta-protein induce acute electrophysiological changes and progressive neurotoxicity in cortical neurons. J. Neurosci. 19, 8876–8884.

Ho, L., Qin, W., Pompl, P.N., Xiang, Z., Wang, J., Zhao, Z., Peng, Y., Cambareri, G., Rocher, A., Mobbs, C.V., Hof, P.R., Pasinetti, G.M., 2004. Diet-induced insulin resistance promotes amyloidosis in a transgenic mouse model of Alzheimer's disease. FASEB J. 18, 902–904.

Hu, Y.S., Xu, P., Pigino, G., Brady, S.T., Larson, J., Lazarov, O., 2010. Complex environment experience rescues impaired neurogenesis, enhances synaptic plasticity, and attenuates neuropathology in familial Alzheimer's disease-linked APPswe/PS1DeltaE9 mice. FASEB J. 24, 1667–1681.

Jankowsky, J.L., Melnikova, T., Fadale, D.J., Xu, G.M., Slunt, H.H., Gonzales, V., Younkin, L.H., Younkin, S.G., Borchelt, D.R., Savonenko, A.V., 2005. Environmental enrichment mitigates cognitive deficits in a mouse model of Alzheimer's disease. J. Neurosci. 25, 5217–5224.

Jankowsky, J.L., Xu, G., Fromholt, D., Gonzales, V., Borchelt, D.R., 2003. Environmental enrichment exacerbates amyloid plaque formation in a transgenic mouse model of Alzheimer disease. J. Neuropathol. Exp. Neurol. 62, 1220–1227.

Jin, M., Shepardson, N., Yang, T., Chen, G., Walsh, D., Selkoe, D.J., 2011. Soluble amyloid {beta}-protein dimers isolated from Alzheimer cortex directly induce Tau hyperphosphorylation and neuritic degeneration. Proc. Natl. Acad. Sci. U. S. A. 108, 5819–5824.

Keller, J.B., Bevier, W.C., Jovanovic-Peterson, L., Formby, B., Durak, E.P., Peterson, C.M., 1993. Voluntary exercise improves glycemia in non-obese diabetic (NOD) mice. Diabetes Res. Clin. Pract. 22, 29–35 [DOI: 10.1016/0168-8227(93)90129-S].

Kitaguchi, H., Tomimoto, H., Ihara, M., Shibata, M., Uemura, K., Kalaria, R.N., Kihara, T., Asada-Utsugi, M., Kinoshita, A., Takahashi, R., 2009. Chronic cerebral hypoperfusion accelerates amyloid beta deposition in APPSwInd transgenic mice. Brain Res. 1294, 202–210.

Lambert, T.J., Fernandez, S.M., Frick, K.M., 2005. Different types of environmental enrichment have discrepant effects on spatial memory and synaptophysin levels in female mice. Neurobiol. Learn. Mem. 83, 206–216.

Laurin, D., Verreault, R., Lindsay, J., MacPherson, K., Rockwood, K., 2001. Physical activity and risk of cognitive impairment and dementia in elderly persons. Arch. Neurol. 58, 498–504.

Lazarov, O., Robinson, J., Tang, Y.P., Hairston, I.S., Korade-Mirnics, Z., Lee, V.M., Hersh, L.B., Sapolsky, R.M., Mirnics, K., Sisodia, S.S., 2005. Environmental enrichment reduces Abeta levels and amyloid deposition in transgenic mice. Cell 120, 701–713.

Lesné, S., Koh, M.T., Kotilinek, L., Kayed, R., Glabe, C.G., Yang, A., Gallagher, M., Ashe, K.H., 2006. A specific amyloid-beta protein assembly in the brain impairs memory. Nature 440, 352–357.

Maesako, M., Uemura, K., Kubota, M., Ando, K., Kuzuya, A., Asada, M., Kihara, T., Kinoshita, A., 2010. Insulin regulates presenilin 1 localization via PI3K/Akt signaling. Neurosci. Lett. 483, 157–161.

Maesako, M., Uemura, K., Kubota, M., Hiyoshi, K., Ando, K., Kuzuya, A., Kihara, T., Asada, M., Akiyama, H., Kinoshita, A., 2011. Effect of glycogen synthase kinase 3 beta-mediated presenilin 1 phosphorylation on amyloid beta production is negatively regulated by insulin receptor cleavage. Neuroscience 177, 298–307.

McClean, P.L., Parthsarathy, V., Faivre, E., Hölscher, C., 2011. The diabetes drug liraglutide prevents degenerative processes in a mouse model of Alzheimer's disease. J. Neurosci. 31, 6587–6594.

Misra, P., 2008. AMP activated protein kinase: a next generation target for total metabolic control. Expert Opin. Ther. Targets 12, 91–100.

Mucke, L., Masliah, E., Yu, G.Q., Mallory, M., Rockenstein, E.M., Tatsuno, G., Hu, K., Kholodenko, D., Johnson-Wood, K., McConlogue, L., 2000. High-level neuronal expression of abeta 1–42 in wild-type human amyloid protein precursor transgenic mice: synaptotoxicity without plaque formation. J. Neurosci. 20, 4050–4058.

Ott, A., Stolk, R.P., van Harskamp, F., Pols, H.A., Hofman, A., Breteler, M.M., 1999. Diabetes mellitus and the risk of dementia: the Rotterdam study. Neurology 53, 1937–1942.

Panza, F., Capurso, C., D'Introno, A., Colacicco, A.M., Del Parigi, A., Seripa, D., Pilotto, A., Capurso, A., Solfrizzi, V., 2006. Diet, cholesterol metabolism, and Alzheimer's disease: apolipoprotein E as a possible link? J. Am. Geriatr. Soc. 54, 1963–1965.

Pedersen, W.A., McMillan, P.J., Kulstad, J.J., Leverenz, J.B., Craft, S., Haynatzki, G.R., 2006. Rosiglitazone attenuates learning and memory deficits in Tg2576 Alzheimer mice. Exp. Neurol. 199, 265–273.

Qiu, W.Q., Folstein, M.F., 2006. Insulin, insulin-degrading enzyme, and amyloid-beta peptide in Alzheimer's disease: review and hypothesis. Neurobiol. Aging 27, 190–198.

Reger, M.A., Watson, G.S., Green, P.S., Wilkinson, C.W., Baker, L.D., Cholerton, B., Fishel, M.A., Plymate, S.R., Breitner, J.C., DeGroodt, W., Mehta, P., Craft, S., 2008. Intranasal insulin improves cognition and modulates beta-amyloid in early. Adv. Neurol. 70, 440–448.

Sanz, C., Gautier, J.F., Hanaire, H., 2010. Physical exercise for the prevention and treatment of type 2 diabetes. Diabetes Metab. 36, 346–351.

Scarmeas, N., Luchsinger, J.A., Mayeux, R., Stern, Y., 2007. Mediterranean diet and Alzheimer disease mortality. Neurology 69, 1084–1093.

Shankar, G.M., Li, S., Mehta, T.H., Garcia-Munoz, A., Shepardson, N.E., Smith, I., Brett, F.M., Farrell, M.A., Rowan, M.J., Lemere, C.A., Regan, C.M., Walsh, D.M., Sabatini, B.L., Selkoe, D.J., 2008. Amyloid-beta protein dimers isolated directly from Alzheimer's brains impair synaptic plasticity and memory. Nat. Med. 14, 837–842.

Solfrizzi, V., Panza, F., Capurso, A., 2003. The role of diet in cognitive decline. J. Neural Transm. 110, 95–110.

Stockley, J.H., O'Neill, C., 2008. Understanding BACE1: essential protease for amyloid-beta production in Alzheimer's disease. Cell. Mol. Life Sci. 65, 3265–3289.

Takasugi, N., Sasaki, T., Suzuki, K., Osawa, S., Isshiki, H., Hori, Y., Shimada, N., Higo, T., Yokoshima, S., Fukuyama, T., Lee, V.M., Trojanowski, J.Q., Tomita, T., Iwatsubo, T., 2011. BACE1 activity is modulated by cell-associated sphingosine-1-phosphate. J. Neurosci. 31, 6850–6857.

Takeda, S., Sato, N., Uchio-Yamada, K., Sawada, K., Kunieda, T., Takeuchi, D., Kurinami, H., Shinohara, M., Rakugi, H., Morishita, R., 2010. Diabetes-accelerated memory dysfunction via cerbrovascular inflammation and Abeta deposition in an Alzheimer mouse model with diabetes. Proc. Natl. Acad. Sci. U. S. A. 107, 7036–7041.

Tandon, A., Rogaeva, E., Mullan, M., St George-Hyslop, P.H., 2000. Molecular genetics of Alzheimer's disease: the role of beta-amyloid and the presenilins. Curr. Opin. Neurol. 13, 377–384.

Walsh, D.M., Klyubin, I., Fadeeva, J.V., Cullen, W.K., Anwyl, R., Wolfe, M.S., Rowan, M.J., Selkoe, D.J., 2002. Naturally secreted oligomers of amyloid beta protein potently inhibit hippocampal long-term potentiation in vivo. Nature 416, 535–539.

Watson, G.S., Cholerton, B.A., Reger, M.A., Baker, L.D., Plymate, S.R., Asthana, S., Fishel, M.A., Kulstad, J.J., Green, P.S., Cook, D.G., Kahn, S.E., Keeling, M.L., Craft, S., 2005. Preserved cognition in patients with early Alzheimer disease and amnestic mild cognitive impairment during treatment with rosiglitazone: a preliminary study. Am. J. Geriatr. Psychiatry 13, 950–958.

Xia, W., Yang, T., Shankar, G., Smith, I.M., Shen, Y., Walsh, D.M., Selkoe, D.J., 2009. A specific enzyme-linked immunosorbent assay for measuring beta-amyloid protein oligomers in human plasma and brain tissue of patients with Alzheimer disease. Arch. Neurol. 66, 190–199.

In Vivo Imaging of Brain Ischemia Using an Oxygen-Dependent Degradative Fusion Protein Probe

Youshi Fujita[1], Takahiro Kuchimaru[2], Tetsuya Kadonosono[2], Shotaro Tanaka[3], Yoshiki Hase[1], Hidekazu Tomimoto[4], Masahiro Hiraoka[5], Shinae Kizaka-Kondoh[2], Masafumi Ihara[1,6]*, Ryosuke Takahashi[1]

1 Department of Neurology, Graduate School of Medicine, Kyoto University, Sakyo-ku, Kyoto, Japan, **2** Department of Biomolecular Engineering, Tokyo Institute of Technology Graduate School of Bioscience and Biotechnology, Nagatsuta-cho, Midori-ku, Yokohama, Japan, **3** Department of Biochemistry, School of Medicine, Tokyo Women's Medical University, Tokyo, Japan, **4** Department of Neurology, Mie University Graduate School of Medicine, Mie, Japan, **5** Department of Radiation Oncology and Image-applied Therapy, Kyoto University Graduate School of Medicine, Shogoin, Sakyo-ku, Kyoto, Japan, **6** Department of Regenerative Medicine and Research, Institute of Biomedical Research and Innovation, Minatojima, Chuo-ku, Kobe, Hyogo, Japan

Abstract

Within the ischemic penumbra, blood flow is sufficiently reduced that it results in hypoxia severe enough to arrest physiological function. Nevertheless, it has been shown that cells present within this region can be rescued and resuscitated by restoring perfusion and through other protective therapies. Thus, the early detection of the ischemic penumbra can be exploited to improve outcomes after focal ischemia. Hypoxia-inducible factor (HIF)-1 is a transcription factor induced by a reduction in molecular oxygen levels. Although the role of HIF-1 in the ischemic penumbra remains unknown, there is a strong correlation between areas with HIF-1 activity and the ischemic penumbra. We recently developed a near-infrared fluorescently labeled-fusion protein, POH-N, with an oxygen-dependent degradation property identical to the alpha subunit of HIF-1. Here, we conduct *in vivo* imaging of HIF-active regions using POH-N in ischemic brains after transient focal cerebral ischemia induced using the intraluminal middle cerebral artery occlusion technique in mice. The results demonstrate that POH-N enables the *in vivo* monitoring and *ex vivo* detection of HIF-1-active regions after ischemic brain injury and suggest its potential in imaging and drug delivery to HIF-1-active areas in ischemic brains.

Citation: Fujita Y, Kuchimaru T, Kadonosono T, Tanaka S, Hase Y, et al. (2012) *In Vivo* Imaging of Brain Ischemia Using an Oxygen-Dependent Degradative Fusion Protein Probe. PLoS ONE 7(10): e48051. doi:10.1371/journal.pone.0048051

Editor: Maria A. Deli, Biological Research Centre of the Hungarian Academy of Sciences, Hungary

Received April 20, 2011; **Accepted** September 24, 2012; **Published** October 19, 2012

Funding: This work was supported by Grants-in-Aid for Young Scientists (B) (to YF) and for Scientific Research (B) (to MI) from the Japanese Ministry of Education, Science, and Culture and by the Global COE Program "Center for Frontier Medicine" funded by the Ministry of Education, Culture, Sports, Science, and Technology (MEXT), Japan. This study is part of a joint research program focusing on the development of technology to establish a Center of Excellence for nanomedicine and carried out by the Kyoto City Collaboration of Regional Entities for Advancing Technology Excellence assigned by the Japan Science and Technology Agency. The funders had no role in study design, data collection and analysis, the decision to publish, or manuscript preparation.

Competing Interests: The authors have declared that no competing interests exist.

* E-mail: iharama@gmail.com

Introduction

Hypoxia-inducible factor 1 (HIF-1) is activated by a variety of stimuli, including focal cerebral ischemia [1]. HIF-1 is a heterodimeric transcription factor consisting of an oxygen-regulated alpha subunit (HIF-1α) and a constitutively expressed beta subunit (HIF-1ß), which play a central role in cellular adaptation by regulating a wide array of genes in response to limited oxygen availability [2]. Under normoxia, prolyl hydroxylases (PHDs) hydroxylate specific proline residues of the oxygen-dependent degradation domain (ODD) of HIF-1α, leading to its polyubiquitination by the von Hippel–Lindau protein (VHL) and subsequent proteasomal degradation. In contrast, hypoxia abrogates prolyl hydroxylation by PHDs and, after VHL binding to HIF-1α, leads to the stabilization and accumulation of HIF-1α [3,4,5].

Oxygenation of brain tissue is impaired as a result of occlusion of a cerebral blood vessel causing subsequent irreversible infarction. The infarct core is surrounded by a hypoxic area [6], known as the ischemic penumbra [7], a region of hypoperfused, functionally impaired, but still viable tissue, in which HIF-1 activation is observed [8,9]. Therefore, the HIF-1-active region in the ischemic brain provides a suitable target for efficiently treating cerebral infarction.

We previously reported that a fusion protein containing the $ODD_{548–603}$ of human HIF-1α is efficiently degraded under normoxic conditions, via a VHL-mediated protein degradation system, in a manner similar to that of HIF-1α [10]. Using ODD-dependent degradation as a target-specific distribution and taking advantage of the capability of the protein-transduction domain (PTD) fusion protein to penetrate the cell membrane, we have developed PTD-ODD fusion proteins that specifically target HIF-1-active cancer cells *in vivo* [11–15]. We recently created a near-infrared fluorescent (NIRF)-labeled PTD-ODD-HaloTag (POH) that functions as an imaging probe specific to HIF-1-active cancer cells both *in vitro* and *in vivo* [16] (Fig. 1). Because NIRF-labeled POH (POH-N) is efficiently delivered to regions with less blood flow [11] and the PTD fusion protein can penetrate the blood–brain barrier [17], POH may be applicable to ischemic brain diseases as a specific probe for detecting HIF-1-active ischemic penumbra.

Here, we investigated the performance of POH-N as a molecular probe for imaging and targeting HIF-1-active regions in an

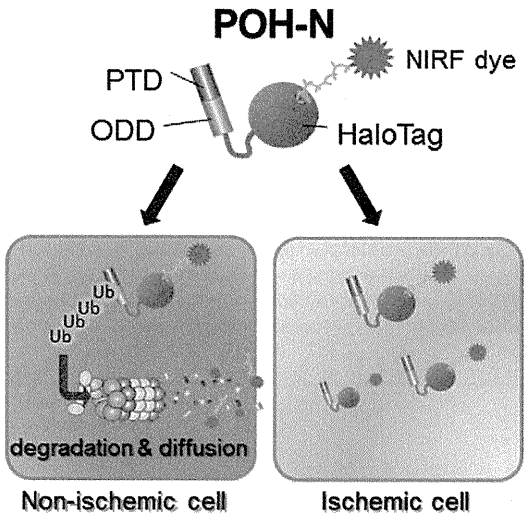

Figure 1. POH-N probe structure. Under normoxic conditions, POH-N is immediately degraded via VHL-mediated ODD, and the resultant POH-N fragments diffuse from the cells. In contrast, POH-N is more stable in HIF-1-active cells, thus creating a contrast between HIF-1-active and HIF-1-inactive cells.
doi:10.1371/journal.pone.0048051.g001

ischemic stroke mouse model. The results demonstrate that POH-N allows *in vivo* monitoring and *ex vivo* detection of the HIF-1-active regions after ischemic brain injury.

Materials and Methods

Ethics statement

All animal experiments in this study were performed with the approval of the Animal Experiment Committees of Kyoto University, Graduate School of Medicine (Permit Number: MedKyo10202) and in strict accordance with the relevant national and international guidelines.

Animal preparation

The cranial window surgical procedure was performed for *in vivo* imaging, as previously described [18]. In brief, male C57BL/6J mice (6–7 weeks old) were anesthetized with 1.5% isoflurane in air, via a snout mask. A 6-mm-diameter hole was made using a fine drill bit in the skull. The center of the cranial window was located 2 mm posterior to the bregma on the midline. The dura mater was left intact. To cover the hole, an 8-mm cover glass (0.45–0.60-mm-thick) was sealed to the skull with histocompatible cyanoacrylate glue and dental cement, which adhered to the bone (Fig. 2A). Transient focal cerebral ischemia was induced using the intraluminal middle cerebral artery (MCA) occlusion (MCAO) technique [19]. Body temperature was maintained at 37°C using a feedback-controlled heating pad. An incision was made into the external carotid artery, and a silicon-coated 8–0 nylon monofilament was inserted through the right internal carotid artery to occlude the MCA at its origin. After 60 min of occlusion, blood flow was restored by withdrawing the nylon suture. For generation of permanent occlusion of MCA, the nylon suture was not withdrawn. The survival rate of the MCAO/R model and the permanent MCAO model was more than 90% 24 hours after operation. Animals were assessed using laser speckle perfusion imaging (Omegazone; Omegawave Inc., Tokyo, Japan) to confirm

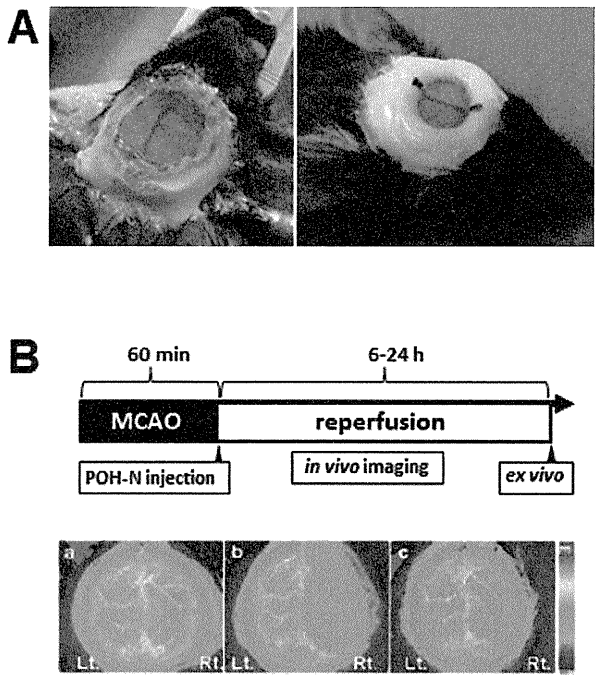

Figure 2. Experimental design. (A) Cranial window in a C57/BL6 mouse. Experimental design of the closed cranial window. (B) Experimental design (upper panel). Representative two-dimensional images of cerebral blood flow measured by laser speckle perfusion imaging before MCAO (a), during MCAO (b), and after reperfusion (c) are shown in the lower panels. MCAO: middle cerebral artery occlusion.
doi:10.1371/journal.pone.0048051.g002

adequate induction of focal ischemia and successful reperfusion (Fig. 2B).

Plasmid construction and preparation of fusion proteins

The plasmid encoding the POH protein was constructed by substituting the coding sequences of procaspase-3 in PTD-ODD-procaspase-3 with HaloTag (Promega, Madison, WI), as previously described [16]. The plasmid encoding POmH containing the point substitution mutation, P564G [15], was prepared using a QuickChange XL site-directed mutagenesis kit (Stratagene, La Jolla, CA) at the proline residue corresponding to HIF-1α P564. Final cDNA constructs were inserted into the pGEX-6P-3 plasmids (GE Healthcare Bio-Science Corp., Piscataway, NJ). Fusion proteins were expressed in BL21-CodonPlus cells (Stratagene, La Jolla, CA) as GST-tagged proteins. These GST-tagged proteins were purified with a GST column and digested with precision protease (GE healthcare Bio-Science Corp., Piscataway, NJ) to remove GST tags from the fusion proteins. The final products were equilibrated in Mg^{2+}/Ca^{2+} free PBS (pH 8.0).

Preparation of the POH-N probe

We used NIRF dye IR800, as previously described [16]. The HaloTag ligand-IR800 was provided by Promega Corporation. HaloTag ligands (1 mg, 2.87 μmol; Promega, Madison, WI) in 100 μL of dimethyl formamide (DMF) were mixed with the NIRF dye and succinimidyl ester (1 mg, ~0.8 μmol; Invitrogen, Carlsbad, CA) in 1 mL of 10 mM boric acid (pH 8.5) in DMF. The reaction mixture was stirred in the dark for 12 h at room temperature. The reaction mixture was applied to a SepPak C18 reverse-phase column (Waters, Milford, MA), and the HaloTag

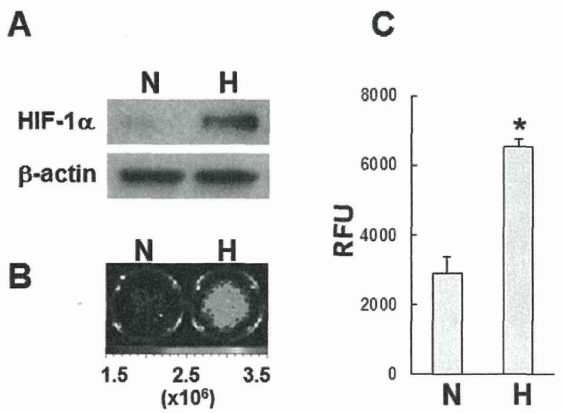

Figure 3. Stabilization of POH-N under hypoxic conditions. SH-SY5Y neuroblastoma cells cultured under normoxic (N) or hypoxic (H) conditions were treated with POH probe. (A) HIF-1α protein levels were analyzed by western blotting (a representative blot is shown). (B) The fluorescence intensity of POH probe in cells was measured. (C) Representative fluorescence images are shown. *$P<0.02$ (vs. normoxic condition).
doi:10.1371/journal.pone.0048051.g003

ligands labeled with NIRF dye (HL-N) were resolved in 100 μL DMF. POH protein (40 μmol/L) was mixed with three volumes of HL-N (120 nmol/15 μL) in 10 mL PBS (pH 8.0) containing 100 mM Tris-HCl (pH 8.0) and 3 M $(NH_4)_2SO_4$ for 2 h. POH-N probes were subsequently purified with a PD-10 gel filtration column (GE healthcare Bio-Science Corp., Piscataway, NJ) and an Amicon-10 centrifugation column (Millipore, Billerica, MA). Purified POH-N was finally resolved in PBS (pH 8.0). Fluorescence characterizations were confirmed by SDS-PAGE fluorescence imaging. The labeling rate, calculated as described by the manufacturer, was >0.7 [16].

In vitro fluorescence measurement

SH-SY5Y neuroblastoma cells (2×10^5 cells/well) were seeded in a six-well plate (Riken Cell Bank, Tsukuba, Japan). The cells were pre-incubated under hypoxic (1% O_2) or normoxic (21% O_2) conditions for 16 h. The probe (500 nM) was then added, followed by incubation for 1 h. The cells were then washed with fresh medium, incubated for 3 h in fresh medium, and suspended in 200 μL of radioimmunoprecipitation assay (RIPA) buffer. Fluorescence was measured and imaged for 150-μL aliquots of suspension in a 96-well plate using an Infinite® F500 microplate reader (Tecan, Durham, NC) with excitation and emission filters at 740±25 and 780±20 nm, and the IVIS®-Spectrum *in vivo* imaging system (Caliper Life Sciences, Alameda, CA) with excitation and emission filters at 710±15 and 800±10 nm, respectively.

Western blot analysis

To analyze cultured cells, SH-SY5Y cells were seeded in a six-well plate. The cells were pre-incubated under hypoxic or normoxic conditions for 6 h, then washed with medium, incubated for 3 h, and lysed using 200 μL of Laemmli sample buffer. Brain tissue samples were homogenized with a Dounce glass homogenizer using ice-cold RIPA buffer supplemented with protease inhibitors (Nacalai Tesque, Kyoto, Japan). Lysates were centrifuged at 10,000× *g* for 10 min at 4°C, and supernatants were collected. Protein concentrations were determined by the BCA protein assay (Pierce, Rockford, IL). Protein samples were electrophoresed on 10% SDS-polyacrylamide gel and transferred to PVDF membranes. The POH-N probes, β-actin and HIF-1α, were detected by a monoclonal anti-β-actin antibody (Sigma-Aldrich, St. Louis, MO) and a polyclonal anti-HIF-1α antibody (R&D Systems, Minneapolis, MN), respectively. The primary antibodies were then reacted with appropriate secondary horseradish peroxidase-conjugated antibodies (GE Healthcare Bio-Science Corp., Piscataway, NJ). Signals were detected using the chemiluminescence ECL-PLUS system (GE Healthcare Bio-Science Corp., Piscataway, NJ). Data were normalized relative to the β-actin levels and expressed as percentages of the sham-operated controls.

In vivo and *ex vivo* fluorescence imaging

POH probe (2 nmol) in 100 μL PBS (pH 8.0) was injected intravenously into the tail vein at 5 min, 6 hours, and 24 hours after reperfusion by the withdrawal of the nylon suture. Alternatively, POH probe (2 nmol) was injected intravenously at 60 min after permanent MCAO, without withdrawal of the nylon suture. Fluorescence images were acquired at the indicated times after injections. All fluorescence images were acquired with the IVIS®-Spectrum (Caliper Life Sciences, Alameda, CA) system, using the following parameters: excitation filter, 710±15 nm; emission filter, 800±10 nm; exposure time, 1 s; binning, small; field of view, 6×6 cm; and f-stop, 1. Some mice were sacrificed after *in vivo* imaging, and their brains were harvested and sliced into 3-mm-thick coronal sections. Fluorescence emissions from these brain sections were measured using the IVIS®-Spectrum

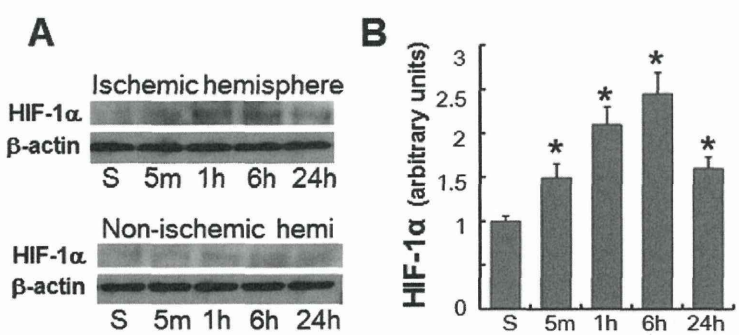

Figure 4. HIF-1α accumulation after focal brain ischemia. (A) Western blot analysis of HIF-1α in the ischemic and non-ischemic hemispheres of mice subjected to MCAO followed by reperfusion. (B) Densitometric analysis of HIF-1α protein levels in the ischemic hemispheres. Data were normalized relative to β-actin levels, and the values obtained from sham-operated controls (S) were arbitrarily defined as 1. *$P<0.05$ (vs. sham, n = 4).
doi:10.1371/journal.pone.0048051.g004

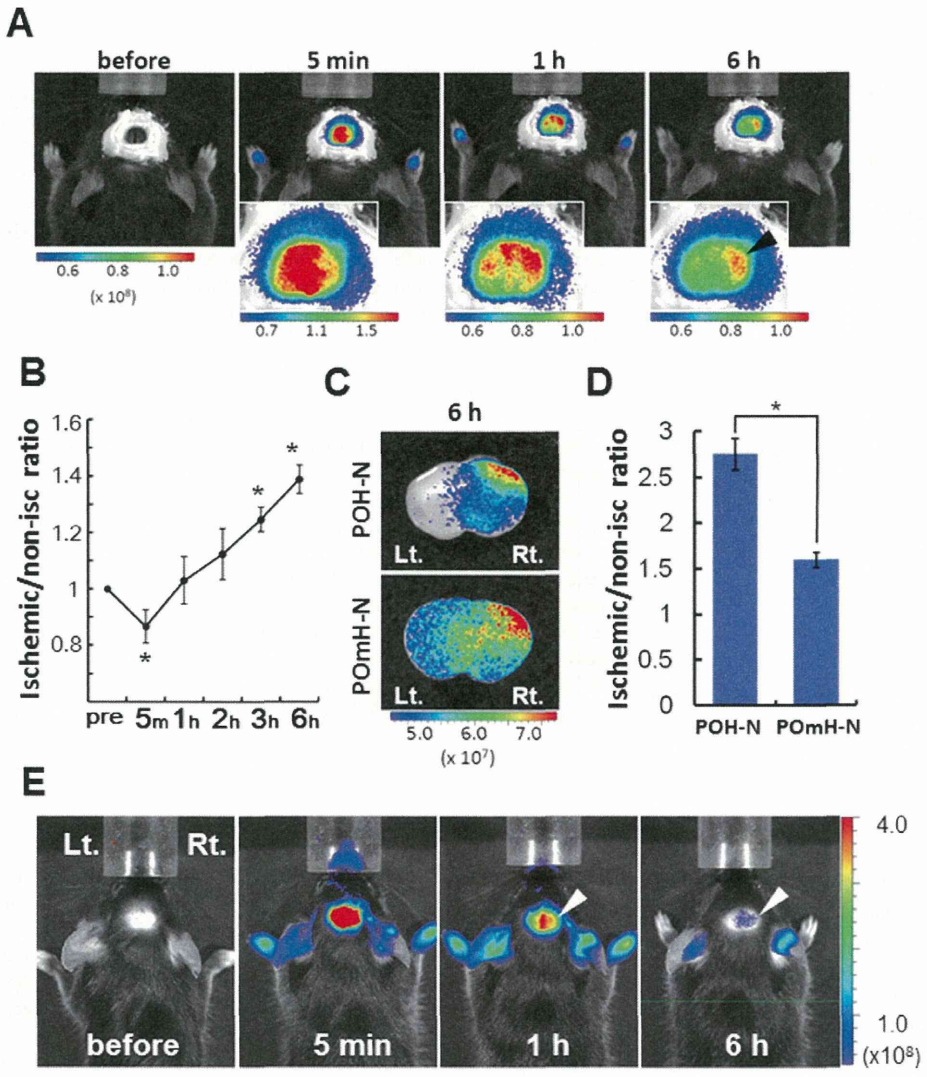

Figure 5. Imaging of HIF-1-active regions in the focal brain ischemia model. (A) Representative *in vivo* fluorescence images visualized through a cranial window before and at 5 min, 1 h, and 6 h after POH-N administration are shown. Magnified head images are shown in the lower left panels. Arrowheads indicate accumulation of the probe in the right ischemic hemisphere. (B) The relative fluorescence intensity of the ischemic hemisphere to the non-ischemic hemisphere. Fluorescence intensities were measured at the indicated times after POH-N administration. $^*P<0.05$, n = 3. (C) *Ex vivo* imaging of the coronal brain sections after POH-N injection. (D) Relative fluorescence of the ischemic hemisphere compared with the non-ischemic hemisphere at 6 h after probe administration (n = 3/group: $^*P<0.05$). Relative fluorescence values were calculated using ROIs mirrored along the midline of the cerebral hemispheres. (E) *In vivo* fluorescence images visualized without preparation of a cranial window before and at 5 min, 1 h, and 6 h after POH-N administration. Anesthetized C57BL/6J mice were shaved and depilated top of the head 24 h before experimentation. Arrowheads indicate accumulation of the probe in the right ischemic hemisphere.
doi:10.1371/journal.pone.0048051.g005

system, under the same set of parameters for the excitation filter, emission filter, and exposure time. Relative fluorescence values were calculated by using regions of interest (ROIs) mirrored along the midline of the cerebral hemispheres. The contribution of the ODD domain in POH to clearance acceleration in the non-ischemic brains was examined using POmH-N, which has a point mutation corresponding to human HIF-1α (P564G) in the ODD domain and thus lacks ODD regulation [20].

Immunohistochemical analyses

Brain cryosections (10-μm-thick) were prepared using a cryostat (Leica CM3050S; Leica Microsystems, Wetzlar, Germany) and fixed in 4% paraformaldehyde. Cryosections were immunolabeled with the following primary antibodies: rabbit polyclonal anti-HIF-1α antibody (R&D Systems, Minneapolis, MN), rabbit polyclonal anti-ODD antibody [16], rabbit polyclonal anti-HaloTag antibody (Promega, Madison, WI), and rabbit polyclonal anti-HSP70 antibody (Cell Signaling Technology, Danvers, MA). Primary antibodies were applied overnight at 4°C. The sections were then incubated with biotin- or FITC-conjugated secondary antibodies. The avidin–biotin–peroxidase complex (ABC) (ABC-Elite; Vector Laboratories, Burlingame, CA) was applied, and the reaction product was visualized using diaminobenzidine (DAB). All photos were taken using a BZ-9000 microscope (Keyence, Osaka, Japan).

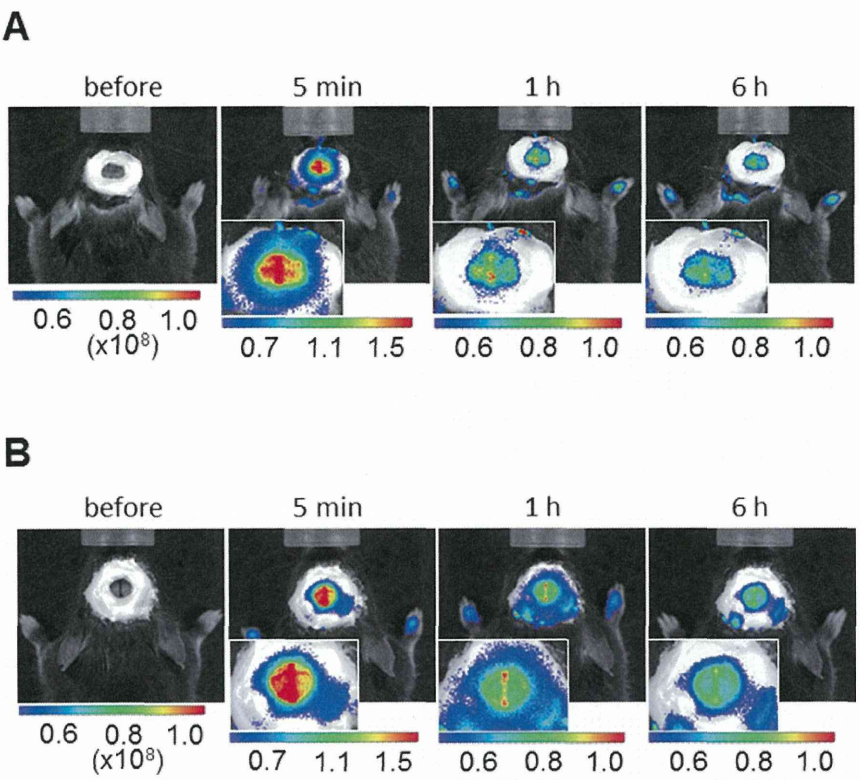

Figure 6. No clear visualization of HIF-1-active regions in the permanent brain ischemia model or with delayed injection of POH-N in the focal brain ischemia model. (A) Representative *in vivo* fluorescence images visualized through a cranial window before and at 5 min, 1 h, and 6 h after POH-N administration are shown. POH-N was injected intravenously at 60 min after permanent MCA occlusion. (B) Representative *in vivo* fluorescence images visualized through a cranial window before and at 5 min, 1 h, and 6 h following POH-N administration at 24 h after reperfusion. Magnified head images are shown in the lower left panels.
doi:10.1371/journal.pone.0048051.g006

Statistical analysis

Data are presented as mean ± SEM. Statistical analyses were performed using ANOVA. Values of $P<0.05$ were considered statistically significant.

Results

Stabilization of POH-N under hypoxic conditions *in vitro*

HIF-1α protein levels increased under hypoxic conditions compared with normoxic conditions (Fig. 3A). When SH-SY5 neuroblastoma cells were treated with POH-N, significantly (*$P<0.02$) higher fluorescent signals were detected in cells cultured in hypoxic conditions compared with normoxic conditions in a manner similar to that of HIF-1α protein levels (Fig. 3B and C).

HIF-1α accumulation after focal cerebral ischemia

Quantitative western blot analysis showed that cerebral ischemia induced by transient MCAO triggered a significant (*$P<0.05$, $n=4$) increase in the HIF-1α protein levels in the ischemic hemisphere (Fig. 4A and B). HIF-1α protein levels reached a peak at 6 h after 60 min MCAO in the ischemic hemisphere and declined thereafter (Fig. 4A and B).

In vivo imaging of HIF-1-active regions in an ischemic stroke model

To examine the possible application of POH-N to ischemic diseases, we administered POH-N in mice with focal cerebral ischemia induced by transient MCAO. The fluorescent signal for POH-N was measured at the indicated times (Fig. 5A and B). Five minutes after POH-N administration, fluorescent signals were lower in the ischemic (right) hemisphere than in the non-ischemic (left) hemisphere, probably reflecting post-ischemic hypoperfusion in the ischemic hemisphere. However, at 1–6 h after POH-N administration, the fluorescence intensity increased in the ischemic hemisphere and decreased in the non-ischemic hemisphere. At 3–6 hours after POH-N administration, the relative fluorescence intensity of the ischemic hemisphere was significantly greater than the baseline, compared to that of the non-ischemic hemisphere (ischemic/non-ischemic ratio) (Fig. 5B).

ODD-dependent clearance acceleration in the non-ischemic brains

Examination of the coronal brain sections confirmed that the fluorescent signal was derived from the ischemic hemisphere, particularly in the cortical region adjacent to the striatum (infarct core), at 6 h after POH-N administration (Fig. 5C). Although the ischemic sites showed higher fluorescence intensity than the non-ischemic sites in both POH-N- and POmH-N-injected brains, the fluorescent signals in POH-N-injected brains were more restricted to the ischemic region (Fig. 5C). Furthermore, the non-ischemic sites in POH-N-injected brains showed significantly lower relative fluorescence intensities than those in POmH-N-injected brains (Fig. 5C and D). The fluorescent signal derived from the ischemic hemisphere was visualized even without cranial window (Fig. 5E).

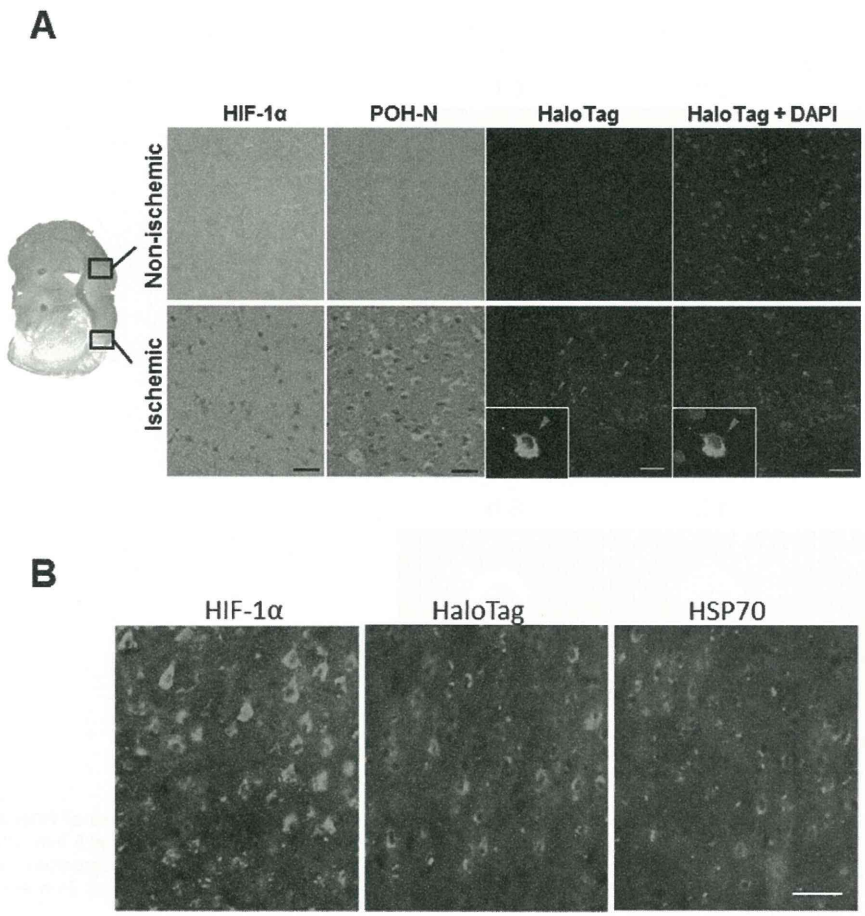

Figure 7. Immunohistochemical detection of HIF-1-active cells and POH-N probe. (A) Immunohistochemical analysis of HIF-1α, POH-N (ODD) and HaloTag (green), with or without DAPI nuclear staining (blue), at 1 day after probe administration. Panels at the bottom show magnified images. (B) Similar distributions of HIF-1α, HaloTag, and HSP70 in pyramidal neurons of the cortical layer bordering the infarct. Scale bars, 50 μm.
doi:10.1371/journal.pone.0048051.g007

However, when POH-N was injected intravenously at 60 min after permanent MCAO or at 24 hours after reperfusion in the transient MCAO, fluorescence intensity was not different between the ischemic and non-ischemic hemispheres (Fig. 6A and B).

Specificity of POH-N to HIF-1α-positive cells in the ischemic brain

Occlusion of the MCA for 60 min induced reproducible ischemic infarcts in the striatum (infarct core) and cerebral cortex, as detected by histology. The specific localization of POH probe in HIF-1-active cells was examined by immunohistochemical analysis of the brain at 24 h after POH-N injection. POH protein was specifically detected in the ischemic cerebral cortex, where abundant HIF-1α-positive cells were also observed (Fig. 7). POH protein was mainly localized to the cytoplasm of cells (magnified images in Fig. 5 bottom panels), which is concordant with a previous report [16]. HIF-1α, HaloTag, and HSP70 showed similar expression patterns in cortical pyramidal neurons within the ischemic penumbra. Overall, these results demonstrate the specificity of POH to HIF-1-active ischemic, but potentially salvageable, cells.

Discussion

In vivo imaging using the POH probe was previously demonstrated to accurately identify HIF-1-active regions in a mouse cancer model [16]. The present study shows that POH-N can also detect HIF-1-active ischemic lesions in a mouse focal cerebral ischemia model. One-hour focal ischemia induced HIF-1 upregulation at 1, 6, and 24 hours post-ischemia, even after reperfusion, probably reflecting the 'no-reflow' phenomenon [21]. Although the tissue in the ischemic hemisphere may have been temporarily subject to relative hyperoxic status after reperfusion, the fluorescent POH system worked at least 24 hours post ischemia, thus enabling HIF-1 imaging. This POH fusion protein method therefore has great potential in improving the diagnosis and treatment of ischemic stroke.

The PTD-mediated delivery system has been demonstrated to enable the delivery of biologically active proteins across the blood–brain barrier. It has been shown that fusion proteins containing the PTD sequence, derived from HIV trans-activator of transcription (TAT), are delivered into the brain tissue after systemic administration [17]. To date, the efficacy of PTD fusion proteins, including the anti-apoptotic protein Bcl-xL, neurotrophic factor GDNF, and antioxidant enzyme SOD, have been demonstrated in rodent models of cerebral ischemia

[22,23,24,25]. However, many neuroprotective drugs that have shown promise in experimental animal models have failed to achieve positive results during clinical trials [26,27]. One of the reasons for such failures is that the target drug levels identified in animals cannot be tolerated by stroke patients. For example, an N-methyl-D-aspartate (NMDA) receptor antagonist has been shown to protect against ischemic stroke at plasma levels greater than 40 μg/mL in animal models; however, the highest tolerable dose in stroke patients is only half of this target level, above which neurological and psychiatric adverse effects are observed [27,28]. One potential way to circumvent such adverse effects would be to take advantage of the ODD-mediated acceleration of clearance under normoxic conditions. In our experiments, POH-N was cleared from the non-ischemic hemisphere significantly faster than POmH-N (Fig. 5). The results strongly support previous reports stating that the ODD domain contributes to the rapid clearance of POH-N from normoxic HIF-inactive tissue [16].

The ischemic penumbra, which is the functionally impaired but potentially viable tissue surrounding the infarct core, is currently considered to be the most promising target for ischemic stroke therapy. However, the accurate identification of patients exhibiting penumbral damage is not straightforward. Currently, the most widely accepted and practical method for identifying the ischemic penumbra in stroke patients is to look for an ischemic region displaying reduced perfusion on MRI but a normal signal on diffusion-weighted imaging [29]. However, several studies show that this interpretation of diffusion- and perfusion-weighted imaging may be an oversimplification [30]. Although the ischemic penumbra was originally defined on the basis of cerebral blood flow and physiological parameters [7], it can also be described in molecular terms [8] by examination of molecular layers emanating from the infarct core. Specifically, pro-apoptotic proteins and anti-apoptotic heat shock protein 70 are expressed in the layer bordering the infarct, and HIF in the layers beyond [31,32,33]. Furthermore, ischemia-induced spreading depression induces the expression of c-fos and many other immediate early genes in the outer layer [34], although such identification methods have not yet been applied in humans.

In the present study, POH-N was delivered to ischemic lesions, including peri-infarct regions (Fig. 7). This result supports the idea that the PTD allows fusion proteins to be delivered to hypoperfused tissue, most likely via diffusion, to achieve the molecular definition of an ischemic penumbra. Furthermore, POH-N significantly accumulated in the ischemic regions and was specifically detected in HIF-1-active cortical cells after focal brain ischemia (Fig. 7). We concede that this imaging technique may be deemed inferior, in terms of resolution, when compared to more established imaging techniques, such as MRI. However, such fluorescent imaging techniques may provide a useful complement to existing imaging techniques, as bedside evaluation would be available without the need of transferring stroke patients to the diagnostic radiology unit. In addition, since HaloTag ligands can be conjugated to a wide range of biomaterials. POH offers a wide range of clinical applications, including the production of imaging probes, even for MRI. Furthermore, a POH-mediated delivery system could be used to selectively target drugs to the ischemic penumbra, an area that has potential for recovery and thus may provide a target for medical interventions.

A limitation that became apparent during this study was the lack of clarity of some images of small mouse brains captured with the IVIS®-Spectrum, which hindered the clear discrimination between ischemic core and penumbra. Another limitation arose through POH-N failing to reach ischemic lesions in the permanent MCAO model. In addition, POH-N had to be injected immediately, not at 6 or 24 hours, after reperfusion to visualize HIF-1-active regions even in the transient MCAO model. Since the partial or complete recanalization rate of major vessel occlusion exceeds 50% in the tPA era [35], clinical application of this *in vivo* fluorescence imaging system should be further explored in parallel with efforts to enhance imaging sensitivity and widen the narrow time window.

Acknowledgments

We are grateful to Yumi Takahashi, Taeko Tani, and Akiko Yoshida for their skilled technical assistance, Takashi Ushiki for technical discussions, Shigeaki Watanabe (Summit Pharmaceuticals International Corporation) for providing technical support regarding IVIS, and Akira Hasegawa and Mark McDougall (Promega Corporation) for their technical advice regarding the HaloTag system. We would also like to thank Maya Uose for secretarial assistance and Ahmad Khundakar for insightful editing of the manuscript.

Author Contributions

Conceived and designed the experiments: YF T. Kuchimaru T. Kadonosono MI SKK. Performed the experiments: YF T. Kuchimaru T. Kadonosono ST YH. Analyzed the data: YF T. Kuchimaru T. Kadonosono ST SKK. Contributed reagents/materials/analysis tools: RT HT MH SKK MI. Wrote the paper: YF SKK MI.

References

1. Bergeron M, Yu AY, Solway KE, Semenza GL, Sharp FR (1999) Induction of hypoxia-inducible factor-1 (HIF-1) and its target genes following focal ischemia in rat brain. Eur J Neurosci 11: 4159–4170.
2. Semenza GL (2000) HIF-1: mediator of physiological and pathophysiological responses to hypoxia. J Appl Physiol 88: 1474–1480.
3. Kaelin WG (2005) Proline hydroxylation and gene expression. Annu Rev Biochem 74: 115–128.
4. Schofield CJ, Ratcliffe PJ (2004) Oxygen sensing by HIF hydroxylases. Nat Rev Mol Cell Biol 5: 343–354.
5. Tanimoto K, Makino Y, Pereira T, Poellinger L (2000) Mechanism of regulation of the hypoxia-inducible factor-1 alpha by the von Hippel–Lindau tumor suppressor protein. EMBO J 19: 4298–4309.
6. Marti HJ, Bernaudin M, Bellail A, Schoch H, Euler M, et al. (2000) Hypoxia-induced vascular endothelial growth factor expression precedes neovascularization after cerebral ischemia. Am J Pathol 156: 965–976.
7. Astrup J, Siesjo BK, Symon L (1981) Thresholds in cerebral ischemia—the ischemic penumbra. Stroke 12: 723–725.
8. Sharp FR, Lu A, Tang Y, Millhorn DE (2000) Multiple molecular penumbras after focal cerebral ischemia. J Cereb Blood Flow Metab 20: 1011–1032.
9. Bergeron M, Yu AY, Solway KE, Semenza GL, Sharp FR (1999) Induction of hypoxia-inducible factor-1 (HIF-1) and its target genes following focal ischaemia in rat brain. Eur J Neurosci 11: 4159–4170.
10. Harada H, Kizaka-Kondoh S, Hiraoka M (2006) Mechanism of hypoxia-specific cytotoxicity of procaspase-3 fused with a VHL-mediated protein destruction motif of HIF-1alpha containing Pro564. FEBS Lett 580: 5718–5722.
11. Harada H, Hiraoka M, Kizaka-Kondoh S (2002) Antitumor effect of TAT-oxygen-dependent degradation-caspase-3 fusion protein specifically stabilized and activated in hypoxic tumor cells. Cancer Res 62: 2013–2018.
12. Harada H, Kizaka-Kondoh S, Hiraoka M (2005) Optical imaging of tumor hypoxia and evaluation of efficacy of a hypoxia-targeting drug in living animals. Mol Imaging 4: 182–193.
13. Harada H, Kizaka-Kondoh S, Li G, Itasaka S, Shibuya K, et al. (2007) Significance of HIF-1-active cells in angiogenesis and radioresistance. Oncogene 26: 7508–7516.
14. Hiraga T, Kizaka-Kondoh S, Hirota K, Hiraoka M, Yoneda T (2007) Hypoxia and hypoxia-inducible factor-1 expression enhance osteolytic bone metastases of breast cancer. Cancer Res 67: 4157–4163.
15. Kizaka-Kondoh S, Itasaka S, Zeng L, Tanaka S, Zhao T, et al. (2009) Selective killing of hypoxia-inducible factor-1-active cells improves survival in a mouse model of invasive and metastatic pancreatic cancer. Clin Cancer Res 15: 3433–3441.
16. Kuchimaru T, Kadonosono T, Tanaka S, Ushiki T, Hiraoka M, et al. (2010) In vivo imaging of HIF-active tumors by an oxygen-dependent degradation protein probe with an interchangeable labeling system. PLoS ONE 5: e15736.